The Astronomical Journal, 164:220 (22pp), 2022 November https://doi.org/10.3847/1538-3881/ac959a

Evidence of Long-term Period Variations in the Exoplanet Transit Database (ETD)

Simone R. Hagey[1], Billy Edwards[2,3,4,5], and Aaron C. Boley[1,6]
[1] The University of British Columbia 6224 Agricultural Road Vancouver, BC V6T 1Z1, Canada; shagey@phas.ubc.ca
[2] AIM, CEA, CNRS, Université Paris-Saclay, Université de Paris, F-91191 Gif-sur-Yvette, France
[3] Blue Skies Space Ltd., 69 Wilson Street, London, EC2A 2BB, UK
[4] Department of Physics and Astronomy, University College London, Gower Street, London, WC1E 6BT, UK
Received 2022 May 30; revised 2022 August 11; accepted 2022 September 9; published 2022 October 27

Abstract

We analyze a large number of citizen science data and identify eight hot Jupiter systems that show evidence for deviations from a constant orbital period: HAT-P-19 b, HAT-P-32 b, TrES-1 b, TrES-2 b, TrES-5 b, WASP-4 b, WASP-10 b, and WASP-12 b. The latter system is already well known to exhibit strong evidence for tidal orbital decay and serves as an important control for this study. Several other systems we identify have disputed period drifts in the literature, allowing the results here to serve as an independent analysis. The citizen science data are from the Exoplanet Transit Database (ETD), which is a global project established in 2008 by the Variable Star and Exoplanet Section of the Czech Astronomical Society. With over 400 planets and 12,000 contributed observations spanning 15 yr, the ETD is brimming with potential for studying the long-term orbital evolution of close-in hot Jupiters. We use our results to discuss prioritization of targets for follow-up investigations, which will be necessary to confirm the period drifts and their causes.

Unified Astronomy Thesaurus concepts: Exoplanets (498); Exoplanet dynamics (490); Transit timing variation method (1710)

Supporting material: machine-readable table

1. Introduction

Hot Jupiters (HJs) are gas giant planets that orbit their host stars with periods less than about 12 days. Their provenance remains debated, although several possible formation pathways exist, such as dynamical excitation followed by tidal circularization (Fabrycky & Tremaine 2007), large-scale disk migration (Lin et al. 1996), and in situ formation (Batygin et al. 2016; Boley et al. 2016). Regardless of how they formed, HJs' proximity to their host stars leads to tidal interactions, which in turn should affect their orbital evolution. Specifically, many HJ orbits should be shrinking gradually over time due to a transfer of angular momentum from the planet to the host star, eventually leading to planetary engulfment (Levrard et al. 2009; Matsumura et al. 2010). This situation occurs when the orbital period of a HJ is shorter than the rotational period of its host star (Penev et al. 2018) or if the angular momentum vectors are antialigned. For a given arrangement, the decay rate can vary depending on the magnitude of stellar tidal dissipation (Levrard et al. 2009; Matsumura et al. 2010). Directly measuring the orbital decay rate provides an estimate of the stellar tidal quality factor Q_*.

While theory predicts many HJs should be decaying, direct detection has remained difficult. Nonetheless, Patra et al. (2020) suggest that certain ensemble properties of HJs indirectly reveal evidence of orbital decay—properties such as the infrequency of planets with periods less than one day, the rapid rotation of some host stars, and the lack of short period planets around such stars.

In principle, careful observations of planetary transit centers over decade timescales should reveal direct evidence for orbital decay (Birkby et al. 2014), appearing as a quadratic timing variation. However, orbital decay is not the only possible scenario for HJ orbital evolution, and some processes cause transit variations that mimic decay. For instance, apsidal orbital precession causes a sinusoidal variation in transit times. Even for fast precession rates, predicted precession periods extend over many decades (Ragozzine & Wolf 2009), making the sinusoidal behavior very difficult to detect. Because of this, the curvature of the transit timing variations (TTVs) from apsidal precession can be consistent with the signal of orbital decay over (relatively) short observing windows. It must be stressed that measuring the apsidal precession rate of a HJ is valuable on its own, as it provides an estimate of the planetary Love number, which enables probing the interior density distribution (Ragozzine & Wolf 2009). Yet other effects may also cause observable transit time variations that do not reflect an inherent change in an HJ's orbit. A line-of-sight acceleration is one such example, in which a wide-orbit companion causes the host star and its HJ to accelerate toward the observer, leading to an apparent decay of the orbital period (Bouma et al. 2020). Stellar activity may also lead to a perceived change in a planet's orbital period on timescales comparable to current HJ observational baselines. A transit light curve is deformed if the planet passes over a starspot, which can affect the fitted transit center time. In the case of persistent starspots, there could be a continuous perturbation of the fitted transit center times. Ioannidis et al. (2016) found that in rare cases this periodic nature could mimic TTVs induced by planetary companions, and Patra et al. (2020) suggest that stellar activity cycles with very long periods could mimic orbital decay. Investigating the effects of stellar activity and line-of-sight

[5] Paris Region Fellow.
[6] Canada Research Chair in Planetary Astronomy.

acceleration on the transit timing of the Exoplanet Transit Database (ETD) targets is beyond the scope of this work but must be considered in follow-up studies.

Whatever the cause, the earliest known HJs have transit observational baselines that span over a decade, making it possible to detect orbital decay or other long-term TTVs. Though many systems of interest have been suggested (see Patra et al. 2020), only WASP-12 b has a clear signature of spiraling into its host star. Indeed, since Maciejewski et al. (2016) first suggested that WASP-12 b does not follow a constant-period ephemeris, the accumulation of more transit and secondary eclipse data has continuously supported an orbital decay model (Patra et al. 2017; Yee et al. 2019; Turner et al. 2020). With the inclusion of observations from the Transiting Exoplanet Survey Satellite (TESS; Ricker et al. 2015), the apsidal precession model has largely been rejected as well (Turner et al. 2020). This work has sparked increased interest within the exoplanet community in searching for decaying HJs, but as of now no other systems have shown such compelling results.

Given the large number of transiting planets that have been discovered, regularly obtaining follow-up observations for each of them has become a difficult task given the limited resources of professional facilities and the perceived low science yield of such observations. However, given their large transit depth, high-quality observations of HJs around bright stars can be achieved with relatively modest equipment. As such, citizen astronomers have for decades been able to observe exoplanetary transits; and importantly, projects such as the ETD, ExoClock (Kokori et al. 2021, 2022), and Exoplanet Watch (Zellem et al. 2020) provide platforms that allow these observers to collectively contribute to cataloging light curves.

Amateur exoplanet transit observations further contribute to updating ephemerides and maximizing observing efficiency at major facilities by ensuring reliable timing. The TESS mission, in particular, has developed the TESS Follow-Up Observing Program to enlist amateur observers to aid in eliminating false positives from TESS exoplanet candidates (Collins 2019). Furthermore, via the ORBYTS program (Sousa-Silva et al. 2018) high-school students have contributed to refining the ephemerides of potential targets for the ESA Ariel mission (Tinetti et al. 2018, 2021) using the Las Cumbres Observatory Global Telescope network of robotic telescopes (e.g., Edwards et al. 2020, 2021). There are also studies in the literature that use select citizen science transits for TTV studies (see, e.g., Baluev et al. 2015; Petrucci et al. 2020; Sonbas et al. 2021). Nonetheless, the exclusive use of such amateur observations are rare, despite their potential for examining long-term orbital changes such as period decay. In this work, we analyze the wealth of citizen scientist observations spanning over a decade in the ETD to demonstrate that these data sets can be used to identify HJ systems that are strong candidates for exhibiting observable orbital evolution. Such selections can then be followed up using large facilities, making efficient use of resources.

In Section 2, we describe the ETD, and in Section 3 we outline our target selection process. Section 4 introduces the transit-timing models and model fitting processes. Our results are presented in Section 5 and discussed in detail, with an emphasis on prospects for future observations in Section 6. This work would not be possible without the hundreds of citizen scientists who submitted transit observations to the ETD, and we ask the reader to take note of the acknowledgments at the end of this paper.

2. Data

The data used in this study are from the ETD. The ETD was established in 2008 by the Variable Star and Exoplanet Section of the Czech Astronomical Society and allows any observer to register and upload transit observations (Poddaný et al. 2010, 2011). As of early 2022, there are 399 planets listed in the database and over 12,000 contributed observations.[7] The website also provides transit predictions and a light curve fitting tool, requiring users to upload their target flux, error, and time stamps. The user is able to upload data with either a geocentric or heliocentric JD format based on the UTC time standard. The fitted transit times are then provided by the database in $\mathrm{HJD_{UTC}}$, which we convert to $\mathrm{BJD_{TDB}}$ for this study. For many systems, there are literature data mixed in with the citizen science observations—one of the initial goals of the ETD project was to have a single space for all amateur and professional transit observations (Poddaný et al. 2010). The inclusion of literature results for any given planetary system in the database is nonetheless incomplete, with the majority posted in the earlier years of the project.

While the database is vast and thus brimming with potential, there are two reasons the ETD is limited in its immediate use: (1) the simplicity of its automatic transit fitting routine and (2) a submission process that allows for inconsistencies in the format of submitted data.

The light curve fitting is done via a Levenberg–Marquardt (L-M) nonlinear least-squares algorithm; namely,

$$m(t_i) = A - 2.5 \log F(z[t_i, t_0, D, b], p, c_1) + B(t_i - t_{\mathrm{mean}}) + C(t_i - t_{\mathrm{mean}})^2, \quad (1)$$

where m_i is the relative magnitudes taken at time t_i, and $F(z, p, c_1)$ is the relative flux, which depends on the radius ratio p, projected planet–star separation z, and limb-darkening coefficient c_1. Stellar limb-darkening is modeled linearly. The projected separation z depends on the mid-transit time t_0, transit duration D, and impact parameter b. Systematic trends in the data are described by B and C, and the zero-point shift of the magnitudes by A. In the fitting algorithm, A, t_0, D, p, B, and C are free parameters. The linear limb-darkening coefficient c_1 is fixed at a value of 0.5 (Poddaný et al. 2010).

Many studies using ETD observations refit the light curves (e.g., Baluev et al. 2015; Mallonn et al. 2019; Davoudi et al. 2021; Edwards et al. 2021). However, the different formats of the observations, both in terms of the machine-readable table format (comma-separated, tab-separated, etc.) and the time stamps provided, make reformatting and refitting the data a very time-consuming process, particularly when assessing a large number of observations. This work involves a total of 4792 transit observations, making refitting the light curves an impracticable course of action in many instances.

Hence, instead of refitting the data, we take the fitted transit centers at face value, as the intent is to show that the ETD, and citizen science more generally, can be an efficient and convenient way to flag planetary systems with nonlinear long-term timing trends.

[7] http://var2.astro.cz/ETD/index.php

The only data categories used in this study are the ETD times, the associated uncertainties on those times, and the epoch numbers. In doing this, there is an implicit assumption that the fitting routine used by ETD does not have a systematic bias and that the time stamps given are in the expected format of HJD_{UTC}. If this is the case, we argue that the main effect of taking the data at face value is to increase the noise. This approach must be used with caution, as the ETD light curve fitting routine is not immune to systematic bias. The L-M algorithm is at higher risk of becoming trapped in a local minimum than a more rigorous Markov Chain Monte Carlo (MCMC) routine, and there is no correction for red noise. Systematic noise in the light curves are modeled quadratically (Equation (1)), though visual inspection of a subset of ETD transits implies that a higher-order approximation may improve the fitting. Additionally, limb-darkening is modeled linearly with a coefficient fixed at a value of 0.5 (Poddaný et al. 2010), which Petrucci et al. (2013) found to be insufficient for the study of short-term TTVs. Despite these potential sources of systematic bias, the agreement of our WASP-12 b analysis with the literature (Section 5) shows that our assumption holds for the purpose of an efficient analysis of potential targets.

The overall quality of observations within the ETD is highly variable. Despite this, when analyzed carefully and consistently, they can be used in independent work and to supplement observations from professional observatories. A good example of the latter is in Kipping & Bakos (2011), who directly compare TrES-2 b transits from the ETD to high-precision Kepler observations of the same epoch number. The ETD observations were found to be in excellent agreement with the Kepler transits, with most of the transit centers matching to within 1σ.

To aid in analyzing the data, transit observations in the ETD are ranked by a "data quality index" (DQ) from 1–5, with 1 being those of the highest quality. The DQ index α is calculated as

$$\alpha = \frac{\delta}{S}\sqrt{\frac{N}{l}}, \tag{2}$$

where δ is the minimum flux, S the mean absolute deviation from the best-fit transit model, N the number of data points, and l the length of the observing run. The greater the value of α, the better quality data. Poddaný et al. (2010) provides the thresholds used for ranking any given observation. For this study, only observations with data quality 1–3 were considered.

3. Target Selection

There are over 400 systems in the ETD,[8] each with varying numbers of observations, data quality, and observational baselines. We are interested in data that might reveal the long-term evolution of planets and, given the range in data quality, focus only on systems that have a large number of observations.

The analysis is restricted to planetary systems that have more than 80 contributed observations with a data quality index of 3 or better. We found that model fits on systems with fewer observations become too dependent on local variations in the data. While there is not a clear transition, and a unique value will not exist, in this scenario a value of 80 removes systems with this strong dependency. Based on this criteria, 30 systems were chosen for further analysis, described further in Section 4. These 30 systems are listed in Table 1.

[8] 404 planets and 12,291 observations as of 2022 May 16.

Table 1
Model Comparison for Initial Analysis of 30 Targets from the ETD

Target	Decay Rate (ms yr^{-1})	1σ Unc. (ms yr^{-1})	BIC_{linear}	BIC_{decay}	ΔBIC
WASP-12 b	−29.1	1.0	2693.4	2284.7	−408.7
TrES-2 b	−20.7	2.1	1334.1	1287.3	−46.8
WASP-10 b	−26.4	2.7	1890.9	1847.9	−43.0
HAT-P-32 b	−30.2	3.3	1084.2	1044.5	−39.7
TrES-5 b	−29.7	3.6	831.6	804.8	−26.8
TrES-3 b	−5.08	0.63	2459.9	2433.2	−26.7
HAT-P-19 b	−55.2	7.2	334.7	308.4	−26.3
TrES-1 b	−7.9	1.4	656.5	646.6	−9.9
XO-2 b	13.0	3.1	490.5	487.1	−3.4
Qatar-1 b	−6.1	1.4	1858.6	1855.3	−3.3
HAT-P-12 b	−13.2	3.6	395.6	393.6	−2.0
GJ-436 b	11.6	3.3	466.5	465.1	−1.4
XO-1 b	−13.3	3.9	265.6	264.5	−1.1
WASP-48 b	−24.6	8.0	426.6	426.4	−0.2
WASP-52 b	−11.8	3.7	513.6	513.4	−0.2
WASP-3 b	−9.0	2.8	503.3	503.2	−0.1
HAT-P-10 b	−15.3	1.8	636.0	636.9	0.9
HAT-P-23 b	−5.2	5.8	435.6	436.5	0.9
HD189733b	2.5	1.1	2452.3	2454.7	2.4
WASP-2 b	−4.2	1.9	641.7	644.3	2.6
HAT-P-20 b	−9.3	4.8	579.4	582.1	2.7
WASP-4 b	−1.09	0.66	356.4	359.1	2.7
HAT-P-36 b	5.0	2.7	1099.5	1103.0	3.5
CoRoT-2 b	2.2	1.7	649.9	653.5	3.6
HAT-P-3 b	−5.1	4.0	755.0	759.0	4.0
GJ-1214b	−0.9	1.8	563.1	567.3	4.2
HAT-P-37 b	6.6	6.8	431.6	435.9	4.2
Qatar-2 b	1.6	2.2	681.4	685.6	4.2
WASP-33 b	−1.4	1.5	2926.9	2931.5	4.6
WASP-43 b	−0.7	1.2	744.7	749.5	4.8

Note. Results from the first run of the analysis pipeline on the raw transit center data of 30 systems from the ETD. Targets are ranked by the likelihood of orbital decay model over a constant-period model. The ΔBIC values are such that a negative value favors the decay model.

4. Methods

A multistep process was used to search for trends in the transit center times. The transit centers are taken directly from the ETD without performing new fits on the individual transit observations. The time stamps, provided by the database in HJD_{UTC}, are converted to BJD_{TDB} for this study following the standard set by Eastman et al. (2010). This conversion is done because, for example, the UTC (Coordinated Universal Time) standard drifts with the addition of leap seconds. Thus, comparing only UTC times that span multiple years may introduce an artificial drift in the transit times that could mimic a true variation in the HJ's orbit. The ETD includes long-term observations of WASP-12 b, which serves as a critical reference due to its comprehensive study in the literature (Maciejewski et al. 2016; Patra et al. 2017; Yee et al. 2019; Turner et al. 2020; Wong et al. 2022). It is thus reassuring that the WASP-12 b results from this study are in agreement with literature values, showing a highly significant decay (Table A9). This alone highlights the value of the ETD observations and suggests that some of the other compelling

targets found in the ETD should be investigated further. Observations of select systems from the database are run through a Python pipeline developed specifically for this project. The data, results, and code used for this project are publicly available on GitHub,[9] and a copy has been deposited on Zenodo: 10.5281/zenodo.7098460.

4.1. Transit-timing models

Three different transit-timing models are tested against the ETD transit centers using MCMC methods. Initial tests were conducted using the *emcee* package (Foreman-Mackey et al. 2013). However, as discussed below, one of the models developed unstable behavior and did not converge in general. To have more direct control over the MCMC algorithm, we implemented a custom Metropolis–Hastings MCMC with a Gibbs sampler (Ford 2006). This latter approach is used for all of the results presented here. For the models, we consider the cases of (1) a planet on a constant orbital period, (2) a planet on a decaying, circular orbit, and (3) a planet that has a constant orbital period, but the orbit is precessing.

In the constant orbital period case, the transit center times increase linearly with the transit epoch E such that

$$t_{\rm tra} = t_0 + \mathrm{PE} \text{ and} \tag{3}$$

$$t_{\rm occ} = t_0 + \frac{P}{2} + \mathrm{PE}, \tag{4}$$

where t_0 is the reference epoch, P is the period, and $t_{\rm tra}$ and $t_{\rm occ}$ are the expected transit and occultation times, respectively.

The second model assumes a steady change in the orbital period with epoch. The simplest expression of this behavior is to include a quadratic term in the expected transit center times. If the fitted period derivative $\frac{dP}{dE}$ is negative, then the planet is decaying. The model is given by

$$t_{\rm tra} = t_0 + \mathrm{PE} + \frac{1}{2}\frac{dP}{dE}E^2 \text{ and} \tag{5}$$

$$t_{\rm occ} = t_0 + \frac{P}{2} + \mathrm{PE} + \frac{1}{2}\frac{dP}{dE}E^2. \tag{6}$$

The third timing model attempts to use apsidal precession to explain timing variations, which requires the HJ orbit to have a nonzero eccentricity—as we will see, even small eccentricities can give rise to measurable effects. To capture the system's behavior in this model, the argument of pericenter ω is assumed to vary at a constant rate, leading to sinusoidal trends in the timing data. Following Patra et al. (2017), the transit and occultation times can be expressed as

$$t_{\rm tra} = t_0 + P_s E - \frac{eP_a}{\pi}\cos\omega, \tag{7}$$

$$t_{\rm occ} = t_0 + \frac{P_a}{2} + P_s E\frac{eP_a}{\pi}\cos\omega, \tag{8}$$

$$\omega(E) = \omega_0 + \frac{d\omega}{dE}E, \text{ and} \tag{9}$$

$$P_s = P_a\left(1 - \frac{d\omega/dE}{2\pi}\right), \tag{10}$$

for argument of pericenter ω, phase ω_0, and precession rate $d\omega/dE$. In these equations, P_s represents the planet's sidereal period, which is assumed to be fixed, while P_a is the "anomalistic" period. This latter period is also fixed but accounts for the additional period signal due to precession.

The MCMC is used to determine the posterior distributions for the model parameters. The constant-period model only has two free parameters: the reference epoch and the period. The decay model has three parameters, adding the dP/dE term. Finally, the apsidal precession model has five parameters: the reference epoch, sidereal period, eccentricity, phase constant, and the precession rate.

Due to the different number of free parameters between the models, the Bayesian information criterion (BIC) is used to compare the relative accuracy and necessity of each model to describe the transit timing data. The BIC is defined as:

$$\mathrm{BIC} = \chi^2 + k\log n, \tag{11}$$

where n is the number of data points, and k is the number of free parameters. Thus, the BIC accounts for the accuracy of the model through the χ^2 statistic, while penalizing the model for the number of free parameters used to describe the data (i.e., the model's complexity). The difference in BIC relates to the Bayesian posterior odds ratio such that a $\Delta\mathrm{BIC} = 10$ corresponds to a 150:1 ratio for the stronger model, and a $\Delta\mathrm{BIC} = 5$ to 13:1 (Liddle 2007).[10] With this in mind, the evidence strongly supports the model with the lower BIC value over the one with the larger value when $\Delta\mathrm{BIC} > 10$. For $5 < \Delta\mathrm{BIC} < 10$, the evidence supports the model with the lower BIC value, and if $\Delta\mathrm{BIC} < 5$, while the lower BIC model is favored, the evidence in support of that distinction is weak.

4.2. Data Cleaning

The transit observations in the ETD are of inconsistent quality and require at least some degree of cleaning. We note above that there is already a numerical data quality factor for each entry in the ETD, which can be used for making an initial selection of data.[11] However, this alone is insufficient due to spurious data points, i.e., points that are well-removed from emergent trends, but with a wide range of reported uncertainties. To address this, an iterative sigma-clipping algorithm is integrated into the MCMC analysis. The process is monitored to avoid introducing an artificial trend in the transit timing curves.

The pipeline begins by finding a preliminary best-fit orbital decay model using 100,000 iterations of the MCMC code. The first 10% of the resulting chain is discarded as burn-in, which is found to be sufficient for the given chain lengths. The resulting preliminary model is subtracted from the timing data. The variance of the residuals is then calculated and used to flag any datum whose nominal value lies outside a 3σ deviation from the residual mean. Another round of fitting is then run, including the MCMC fitting, but with the flagged data excluded. This process is repeated until no points fall outside of the 3σ range. Convergence is achieved on average after 3.6 iterations with an average number of observations removed. After this is complete a final, longer run of the MCMC is performed for the orbital decay model (5,000,000

[9] https://github.com/simonehagey/ExoPdot

[10] It is important to note that the BIC is one of many valid model comparison statistics.

[11] As a reminder, we automatically remove transit centers that have an associated data quality factor of 4 and 5 (1 is the best, and 5 is the worst).

iterations with 10% discarded as burn-in) and, if desired, the precession model.

A worry of using the sigma-clipping method is that it may introduce a false signal, a potential issue that was recognized early on. To address this, during development of the fitting routines, the same overall method was tried but with a best-fit linear model subtracted from the data instead of the best-fit orbital decay model. It was found that the fitted parameters from both methods agreed within respective uncertainties and that the most likely timing model for any given system remained the same. Essentially, data that are better described by a linear trend just resulted in a quadratic best-fit model with very low curvature, and we did not "clip" the data into a quadratic trend. Given comparable results, we decided to focus on using the decay model for the sigma-clipping because it would be, in principle, more sensitive to trend detection. However, the linear model subtraction approach is still run to confirm strong timing trends and discussed as appropriate.

4.3. Model Fitting Approach

The data analysis pipeline described above is applied twice in total. For the first application, each of the 30 star–planet systems selected from the ETD (see Section 3) are processed in the pipeline. During this run, all transit centers that have a DQ of 1, 2, or 3 are included in model fitting. Eight systems show evidence of a nonlinear trend (Table 1) and are investigated further. Two additional targets are included due to potential nonlinear trends being previously reported in the literature (and with different studies reporting inconsistent results): WASP-4 b (see Baluev et al. 2019, 2020; Bouma et al. 2019, 2020; Southworth et al. 2019; Ivshina & Winn 2022; Turner et al. 2022) and WASP-43 b (see Blecic et al. 2014; Chen et al. 2014; Murgas et al. 2014; Ricci et al. 2015; Hoyer et al. 2016; Jiang et al. 2016; Zhao et al. 2018).

The resulting 10 systems are then manually cleaned before being run through the data pipeline a second time. This is a time-consuming process, which is why it is only done at this stage. Specifically, any observation in the database without a clear transit or a clear ingress and egress are manually flagged and excluded from further analysis. Entries without a reported uncertainty are also excluded, automatically. Because this project purposefully does not involve refitting light curves, manual data inspection is necessary to filter out transits without clearly defined edges. It also demonstrates that relying on the DQs alone is insufficient, despite the intended use of DQs. For example, Poddaný et al. (2010) state that partial transits uploaded to the ETD would automatically be given a data quality index of 5, but this automated flagging appears to have stopped after some time. The transit observations that are included in these cleaned data sets are available in Table B1 for reproducibility. With these 10 systems now having been manually cleaned, the data are run through the pipeline a second time. At this point, the apsidal precession model is also included.

The orbital decay model fitting is well-behaved and consistently converges to a clear solution. Uniform prior distributions are placed on the three free parameters (t_0, P, and dP/dE) and a wide parameter space can be explored. Fitting the precession model, however, proved to be nontrivial due to degeneracies between viable models, which we attribute to be due, in part, to the high variance of the data. In particular, the anticorrelations between the eccentricity, e, and the precession rate, $d\omega/dE$, as well as between e and the reference transit time, t_0, lead to posterior solutions that show two or more strong peaks. After exploring many options, a selection of priors and bounds on parameters was determined to be necessary to derive converged results. Indeed, it is this issue that ultimately led to writing a custom MCMC routine. To ensure convergence of our posterior chains, we examined a number of outputs such as trace plots, corner plots, and the autocorrelation coefficient as a function of the lag, all of which are consistent with convergence.

Table 2 summarizes the prior distributions and bounds placed on the parameters for all three transit-timing models. A normal distribution prior is placed on the period, centered on the best-fit result from the constant-period model fit. This is justified by the observation that this constant period can be viewed as an analog for the sidereal period in the apsidal precession model (Equation (10)). A uniform prior distribution is appropriate for ω_0, and log-uniform priors are used for e and $d\omega/dE$ to account for the wide range of possible parameter space.

Without placing a formal bound on the precession rate, the model tends to go to high frequencies in an attempt to fit the datum-to-datum variation, an unphysical situation. To address this, we use the results of Ragozzine & Wolf (2009), who estimate that WASP-12 b should have a precession rate of 19 deg yr^{-1} (roughly 0.001 radian epoch^{-1}). Out of all of the systems they studied, WASP-12 b has by far the highest predicted rate. With this in mind, an upper bound of 0.001 radian epoch^{-1} is placed on $d\omega/dE$ for all systems, even for WASP-12 b, as a higher bound on the precession rate does not result in a better fit to the data in this case (tests using a higher bound for WASP-12 b were conducted to confirm this result). A lower bound of 1×10^{-6} rad epoch^{-1} is also chosen to avoid the M-H algorithm becoming trapped in a local minimum, as very low values of $d\omega/dE$ and e cause the fitted precession model to approach a line even when the results of the orbital decay model indicate the presence of curvature in the data. The eccentricity is restricted to be less than 0.1, which is appropriate for the HJ population and greater than 1×10^{-5}. Ragozzine & Wolf (2009) found that even eccentricities on the order of 10^{-5} can result in detectable TTVs, though measurements of eccentricities are essentially unconstrained by 10^{-3}.

The strictest requirement for convergence of the apsidal precession model is on the parameter bounds of the reference transit center time t_0. The parameter t_0 is allowed to be within a range of ± 0.01 (just over 30 minutes) or ± 0.1 day around the best-fit value from the constant-period model, depending on the system. This final adjustment allows convergence on the solution, but only as a perturbation of the constant-period case. To aid convergence, a nonlinear least-squares fit (*scipy* implementation) of the precession model was done within these bounds to select the best initial value of the model parameters. Altogether, this procedure facilitates convergence of the precession models with the given data sets, and with all of this in mind, we next discuss the results.

5. Results

As noted above, the first run of the analysis pipeline includes all DQ 1–3 observations from all 30 of the initial targets (see Section 3). Table 1 ranks the star–planet systems by the difference in their Bayesian information criterion (ΔBIC), with

Table 2
MCMC Priors

Parameter	Symbol	Unit	Prior	Bounds
Constant period				
Transit center	t_0	$\mathrm{BJD_{TDB}}$	Uniform	$(t_{\mathrm{ref}} - 0.5,\ t_{\mathrm{ref}} + 0.5)$
Period	P	days	Uniform	$(P_{\mathrm{ref}} - 0.5,\ P_{\mathrm{ref}} + 0.5)$
Orbital decay				
Transit center	t_0	$\mathrm{BJD_{TDB}}$	Uniform	$(t_{\mathrm{best}} - 0.5,\ t_{\mathrm{best}} + 0.5)$
Period	P	days	Uniform	$(P_{\mathrm{best}} - 0.5,\ P_{\mathrm{best}} + 0.5)$
Decay rate	dP/dE	days epoch^{-1}	Uniform	$(-1 \times 10^{-7},\ 1 \times 10^{-7})$
Apsidal precession				
Transit center	t_0	$\mathrm{BJD_{TDB}}$	Uniform	$(t_{\mathrm{best}} - a,\ t_{\mathrm{best}} + a),\ a \in \{.01,\ .1\}$
Sidereal period	P_s	days	Normal	$(P_{\mathrm{best}} - 0.1,\ P_{\mathrm{best}} + 0.1)$
Argument of periastron	ω_0	rad	Uniform	$(0,\ 2\pi)$
Precession rate	$d\omega/dE$	rad epoch^{-1}	Log-uniform	$(1 \times 10^{-6},\ 1 \times 10^{-3})$
Eccentricity	e		Log-uniform	$(1 \times 10^{-5},\ 1 \times 10^{-1})$

Note. Parameters t_{ref} and P_{ref} are the reference ephemeris from the literature, whereas t_{best} and P_{best} are the best-fit values from sampling the constant-period model. For the constant-period and orbital decay models the bounds on t_0 and P are generous to allow for exploration of a large parameter space, as there were no issues with converging on multiple solutions. The restrictions on the apsidal precession priors are discussed in Section 4.3.

Table 3
Model Comparison for Secondary Analysis of Top 10 Targets

Target	Decay Rate (ms yr^{-1})	1σ Unc. (ms yr^{-1})	$\mathrm{BIC_{linear}}$	$\mathrm{BIC_{decay}}$	ΔBIC	$\mathrm{BIC_{precession}}$
WASP-12 b	−31.6	1.0	2353.1	1911.8	−441.3	1929.4
WASP-4 b	−6.21	0.70	404.9	369.5	−35.4	378.8
WASP-10 b	−21.9	2.4	1011.3	976.0	−35.3	984.6
HAT-P-19 b	−57.7	7.3	270.4	243.1	−27.3	251.5
TrES-5 b	−34.5	4.6	541.1	518.9	−22.2	529.0
TrES-1 b	−10.9	2.0	190.9	181.2	−9.7	190.2
TrES-2 b	−12.6	2.4	878.9	870.6	−8.3	882.4
HAT-P-32 b	−7.3	1.5	677.2	669.8	−7.4	679.2
TrES-3 b	−2.75	0.78	939.8	938.9	−0.9	982.7
WASP-43 b	−1.0	1.2	576.2	580.6	4.4	593.1

Note. Transit-timing model comparison for the second run of the analysis pipeline on the reduced data of the top 10 systems of interest. The ΔBIC is calculated for the comparison of the constant-period and orbital decay transit-timing models, where a negative value favors the latter. The BIC values for the apsidal precession model fits are provided for further comparison.

a negative value favoring the decay model. The best-fit period decay rates, along with the corresponding 1σ uncertainties, are given in ms yr^{-1}. For some systems, such as GJ-436 b and XO-2 b, the period derivative is positive. In such cases, we found the scatter in the data to be very high, and did not investigate such systems further in this study. They will nonetheless need to be examined in future studies as better data are acquired.

From Table 1, the top eight candidates from this first analysis are selected for the second, deeper analysis described in Section 4.3. Those top eight candidates, in order of evidence for decay, are WASP-12 b, TrES-2 b, WASP-10 b, HAT-P-32 b, TrES-5 b, TrES-3 b, HAT-P-19 b, and TrES-1 b. With the exception of TrES-1 b, all of these systems yield a $\Delta\mathrm{BIC} > 10$ (Section 4.1). The evidence for TrES-1 b is still compelling, with $\Delta\mathrm{BIC} = 9.9$. In addition to these eight targets, WASP-4 b and WASP-43 b are selected due to their relevance in the literature, for a total of 10 targets.

The results of the second round of analysis are summarized in Table 3. In the following subsections, each of these star–planet systems is presented individually, with an expanded discussion of that system's model fitting. The cleaned data sets for the top 10 systems are further provided in the tables listed in Table B1, including the epoch number, transit centers, and respective uncertainty, data quality index, and observer name(s). The full MCMC outputs from the analyses can be found in the tables in Appendix A, which include the best-fit model parameters and their 1σ uncertainties, as well as metrics such as the χ^2, number of data, etc.

Out of the eight highest-ranked systems from Table 1, all but TrES-3 b maintain statistically significant evidence of orbital decay in the ETD transit centers. WASP-4 b and WASP-43 b, both of which favored a constant-period transit-timing model in the first analysis (Table 1), exhibit varying results. For WASP-43 b, the second analysis maintains that the planet's transits follow a linear ephemeris (see Section 5.10), whereas for WASP-4 b the favored model changes to orbital decay with a decay rate of -6.21 ± 0.70 ms yr^{-1} (see Section 5.2).

As a cautionary approach, the secondary analysis was repeated under the assumption that the transit center uncertainties in the ETD are underestimated, thus replacing them with the standard deviation of the spread of the timing residuals—i.e., the observed transit centers minus the times calculated from the best-fit linear ephemeris. In general, using a nonlinear least-squares algorithm can lead to optimistic parameter uncertainties. In addition, when describing the ETD light curve fitting routine, Poddaný et al. (2010) acknowledge that the

Table 4
Model Comparison for Secondary Analysis—Data Variance for ETD Transit Times

Target	Decay Rate (ms yr^{-1})	1σ Unc. (ms yr^{-1})	BIC$_{\rm linear}$	BIC$_{\rm decay}$	ΔBIC
WASP-12 b	−34.8	4.9	223.7	202.7	−21.0
HAT-P-19 b	−64	17	80.6	78.2	−2.4
TrES-1 b	−16.0	3.7	73.3	68.3	−5.0
WASP-4 b	−6.7	2.4	62.6	62.7	0.1
TrES-2 b	−22.0	8.0	159.0	160.3	1.3
TrES-5 b	−25	11	118.3	120.5	2.2
HAT-P-32 b	−32	12	95.5	96.7	1.2
WASP-10 b	−10.1	7.6	131.6	135.5	3.9
WASP-43 b	3.5	4.0	126.5	130.9	4.4
TrES-3 b	0.01	1.9	227.8	233.1	5.3

Note. Model comparison of the results from the reduced data of the top 10 systems after replacing the ETD transit center uncertainties with the standard deviation of the nominal timing residuals. A negative ΔBIC value favors the orbital decay model.

errors of their L-M fit may be underestimated due to the lack of red noise correction and a fixed impact parameter. Substituting the ETD uncertainties in this way allow for an examination of the curvature in the data unbiased by the uncertainties given by the ETD light curve fitting tool (Table 4).

It is notable that, with the exception of HAT-P-32 b and WASP-10 b, all of the resulting decay rates agree within the respective uncertainties with those in Table 3. However, as to be expected, the uncertainties are much larger, and only three systems (WASP-12 b, HAT-P-19 b, and TrES-1 b) still exhibit statistical evidence for departure from a linear ephemeris, using a fixed variance of the data (Table 4).

5.1. WASP-12 b

WASP-12 b is a 1.4 $M_{\rm J}$, 1.8 $R_{\rm J}$ HJ discovered in 2008 on a 1.09142090 ± 0.0000002 days orbit (Hebb et al. 2008; Bonomo et al. 2017). The TTVs of WASP-12 b have been extensively studied, as it is the only exoplanet for which orbital decay has been unambiguously detected. The first suggestion of a period drift was from Maciejewski et al. (2016), who found that the WASP-12 b transit times diverged from a linear ephemeris. Various studies have since confirmed this finding, all with compatible decay rates (see, e.g., Patra et al. 2017; Yee et al. 2019; Turner et al. 2020), the most recent result being -30.27 ± 1.11 ms yr^{-1} from Ivshina & Winn (2022).

At the time of writing, the ETD hosts 295 observations of WASP-12 b spanning the years 2008 to 2021, 257 of which have DQ 1–3. The curvature of the transit timing residuals is clear when looking at the ETD generated $O-C$ plot.[12] Prior to any data cleaning, the ETD transit times fit an orbital decay model with a period derivative of -29.1 ± 1.0 ms yr^{-1}, preferred over a linear ephemeris by ΔBIC of 408.7 (Table 1). This is by far the greatest ΔBIC of all of the targets, with the next best being 46.8 for TrES-2 b.

After removing partial and duplicate transits, 218 WASP-12 b transit times remain (Table B1), five of which are from published literature studies. The final analysis of the cleaned WASP-12 b data increases the ΔBIC to 441.3 favoring orbital decay at a rate of -31.6 ± 1.0 ms yr^{-1} (see Figure 1). The quadratic trend is also favored over apsidal precession by a ΔBIC of 17.6. The best-fit precession rate is $0.000336^{+0.000026}_{-0.000013}$ rad per epoch with an eccentricity of $0.0287^{+0.0022}_{-0.0039}$ (Table A9).

[12] http://var2.astro.cz/ETD/etd.php?STARNAME=WASP-12&PLANET=b

5.2. WASP-4 b

HJ WASP-4 b has an orbital period of $1.338231624 \pm 0.000000068$ days and a radius and mass of 1.42 $R_{\rm J}$ and 1.22 $M_{\rm J}$, respectively (Wilson et al. 2008; Bonomo et al. 2017). The first suggestion of a period variation in WASP-4 b in the literature was from Bouma et al. (2019), who added 18 TESS transits to a collection of observations going back to 2007 and found the period to be changing at a rate of -12.6 ± 1.2 ms yr^{-1}. Later in the same year, Southworth et al. (2019) included their own data from the years 2009–2019 and found that WASP-4 b is decaying at a rate of -9.2 ± 1.1 ms yr^{-1}, while Baluev et al. (2019) conducted a homogeneous analysis and found no statistically significant evidence of a nonlinear timing trend. In 2020, Baluev et al. (2020) detected a nonlinear trend with 3.4σ significance and Bouma et al. (2020) reported a period change of -8.64 ± 1.26 ms yr^{-1} for WASP-4 b from transit observations. However, after an analysis of new radial velocity data, they found that the Doppler effect from WASP-4 b accelerating toward the Earth has the effect of decreasing the period by -5.94 ± 0.39 ms yr^{-1}. Thus, they conclude the period change is "mostly or entirely" due to acceleration of the system along the line of sight (Bouma et al. 2020). However, a recent comprehensive analysis from Turner et al. (2022) did not detect this acceleration in the RV data, instead finding evidence of an additional planet in the system with a period of approximately 7000 days in addition to TTVs that are consistent with orbital decay at a rate of -7.33 ± 0.71 ms yr^{-1}. Another recent study from Ivshina & Winn (2022) measured the period of WASP-4 b to be changing at a compatible rate of -5.81 ± 1.58 ms yr^{-1}.

Like WASP-43 b, WASP-4 b was selected for further investigation in this study because of this interest in the literature. The ETD lists 68 transit observations of WASP-4 b from the years 2009–2021, 63 of which are DQ 1–3. As many of the transits are high quality, this is a valuable resource for contributing to our understanding of the WASP-4 star–planet system. The initial analysis of the ETD transit centers does not support a departure from a linear ephemeris, with the ΔBIC favoring the constant-period model by 2.7 and the best-fit decay rate being -1.09 ± 0.66 ms yr^{-1} (Table 1). After the exclusion of partial and duplicate transits for the second analysis, 55 observations of WASP-4 b remain (Table B1), 10 of which are from published literature studies.

The analysis of the cleaned WASP-4 b data changes the favored transit-timing model (Figure 1). In the second analysis, orbital decay at a rate -6.21 ± 0.70 ms yr^{-1} is strongly favored for WASP-4 b over the constant-period model by a ΔBIC of 35.4 (Table 3). The apsidal precession model is also a clear contender by a ΔBIC of 26.1 when compared to a constant period, but orbital decay is still strongly favored over precession by $\Delta{\rm BIC} = 9.3$. The best-fit precession rate is $0.00048^{+0.00040}_{-0.00024}$ with an eccentricity of $0.0027^{+0.0079}_{-0.0017}$ (Table A7). This study does not evaluate the likelihood or directly model a line-of-sight acceleration of the WASP-4 b system, but in this context, the orbital decay rate can be treated as a constant period derivative within a different physical context. Whatever the underlying reason, the evidence in the data support a timing variation.

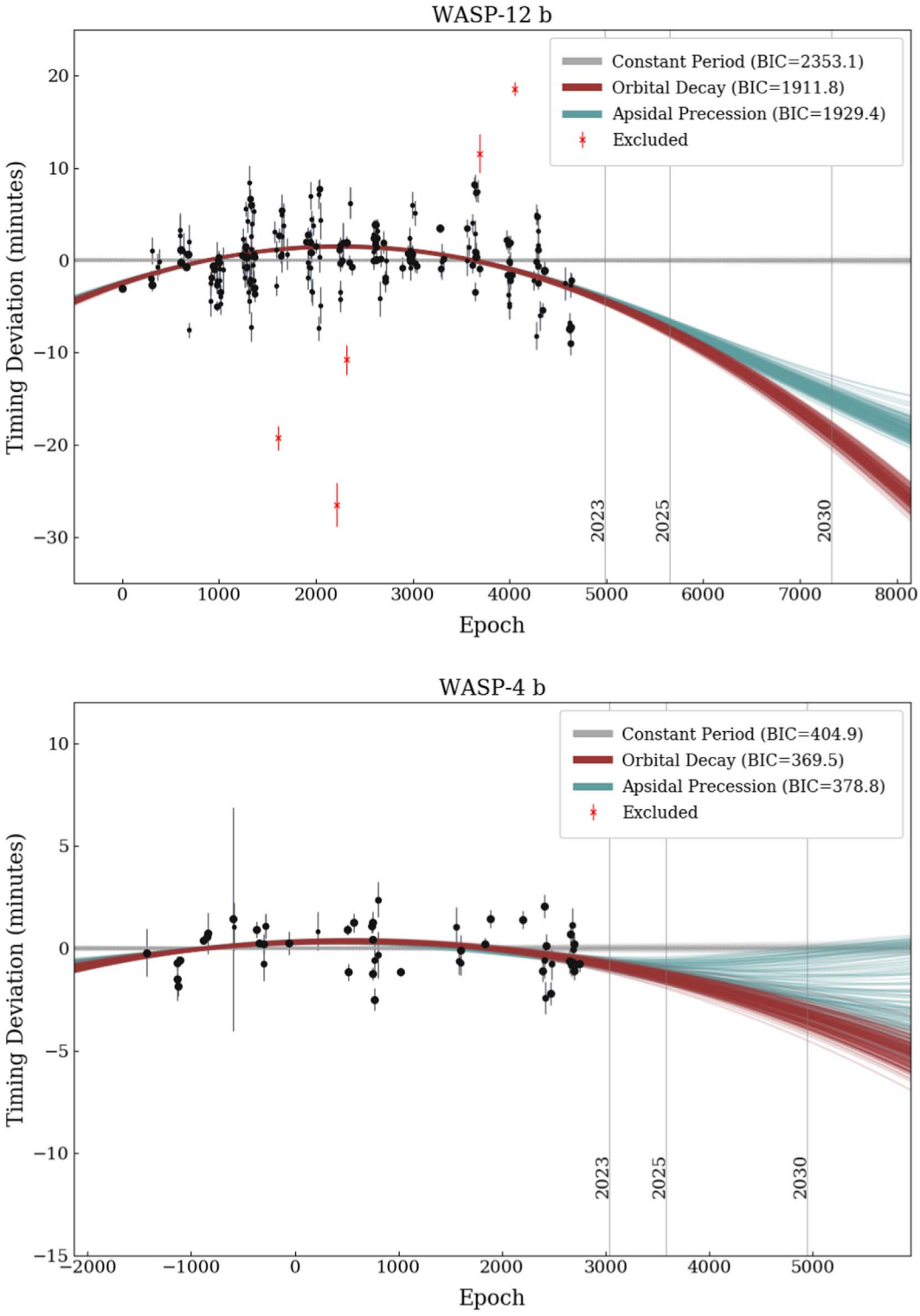

Figure 1. Timing residuals of WASP-12 b (top) and WASP-4 b (bottom) with future projections of the three transit-timing models shown with 150 random draws from the MCMC posterior chains. Note that for esthetic reasons, the scaling of the *y*-axis varies for each plot. Each datum is the difference between an observed time and the time predicted by the best-fit constant-period model. The size of the data points correspond to the data quality index from 1 to 3, with the higher-quality transits being larger. The red crosses represent observations removed during the sigma-clipping process.

5.3. WASP-10 b

WASP-10 b is a 3.2 M_J, 1.1 R_J HJ discovered on a $3.09272932 \pm 0.00000032$ days orbit in 2009 (Christian et al. 2009; Bonomo et al. 2017). It has been the subject of multiple timing studies in the past due to a measured periodic TTV, with proposed explanations including starspot occultations (Barros et al. 2013) and a 0.1 M_J companion with a period of about 5.23 days (Maciejewski et al. 2011a, 2011b). A second planet in the system has never been confirmed, and we have not found further discussion in the literature of other studies looking for

long-term trends in the transit times of WASP-10 b, such as orbital decay or apsidal precession.

The ETD hosts 202 observations of WASP-10 b spanning the years 2007–2021, 174 of which are DQ 1–3. An initial examination of the WASP-10 b data gave a best-fit orbital decay rate near -130 ms yr^{-1}, largely driven by a single data point from Johnson et al. (2009). Removing this observation from the data set gave a more conservative period derivative of -26.4 ± 2.7 ms yr^{-1}, which is the value reported in the initial round of analyses (Table 1). WASP-10 b was selected for further analysis, with the orbital decay model being strongly favored over a constant period by a ΔBIC of 43.0.

During the data reduction process it was revealed that the observation in Johnson et al. (2009) was corrected in an erratum (Johnson et al. 2010). In addition to this, the transit centers published in Christian et al. (2009) and Maciejewski et al. (2011a) had to be converted to BJD_{TDB} from BJD_{UTC} and BJD_{TT}, respectively. After removing all partial and duplicate transits, there are 129 observations of WASP-10 b remaining, including 19 measurements from the literature (Table B1). The final analysis of the cleaned WASP-10 b data retained the strong preference for the orbital decay model (Figure 2) by a ΔBIC of 35.3 with a best-fit decay rate of -21.9 ± 2.4 ms yr^{-1} (Table 3). The apsidal precession model is also a better fit to the data than a constant period, but orbital decay is favored by ΔBIC of 8.6. The best-fit apsidal precession model gives an eccentricity $0.0037^{+0.0027}_{-0.0011}$ and precession rate $0.00078^{+0.00015}_{-0.00020}$ rad per epoch (Table A8).

5.4. HAT-P-19 b

HAT-P-19 b is a Saturn-mass (0.29 M_J) planet with a 1.1 R_J radius on a 4.008778 ± 0.000006 days orbit (Hartman et al. 2011a; Bonomo et al. 2017). In the discovery paper, Hartman et al. (2011a) detected a linear trend in the radial velocity residuals, indicating the presence of a another body in the planetary system. This observation led to multiple studies seeking periodic TTVs (Seeliger et al. 2015; Maciejewski et al. 2018; Bastürk et al. 2020), but we have not found further discussion in the literature on testing for long-term trends in the timing residuals.

HAT-P-19 b was selected as a target of interest after the first round of analyses showed a preference for orbital decay (ΔBIC = 26.3) at a rate of -55.2 ± 7.2 ms yr^{-1} (Table 1). The ETD has 98 observations of HAT-P-19 b spanning the years 2009–2021, 88 of which are DQ 1–3. The only literature observation is the discovery epoch, which had to be converted from BJD_{UTC} to BJD_{TDB} (Hartman et al. 2011a). After the exclusion of partial and duplicate transits, 75 observations of HAT-P-19 b remain (Table B1). The second analysis of HAT-P-19 b on this cleaned data set (Figure 2) yields a period derivative of -57.7 ± 7.3 ms yr^{-1}, this time favoring the decay model by a ΔBIC of 27.3 (Table 3). The orbital decay model is also favored over apsidal precession by a ΔBIC of 8.4. The best-fit precession model yields an eccentricity of $0.0068^{+0.0009}_{-0.0010}$ and a precession rate of $0.000905^{+0.000059}_{-0.000068}$ rad per epoch (Table A1).

5.5. TrES-5 b

TrES-5 b is a 1.8 M_J, 1.2 R_J HJ discovered in 2011 on a $1.48224460 \pm 0.00000070$ days orbit (Mandushev et al. 2011; Bonomo et al. 2017). The first suggestion of TTVs in the literature was by Sokov et al. (2018), who detected periodic timing variations indicative of a second planet in the system with a mass of 0.24 M_J in the 1:2 resonance orbit. Maciejewski et al. (2021) were not able to confirm or reject the existence of an additional body in the system via short-term TTVs. However, they found a long-term variation in the orbital period of -20.4 ± 4.7 ms yr^{-1} and conclude it is most likely a line-of-sight acceleration of the system induced by a massive, wide-orbiting companion. At the time of writing, the most recent timing study of TrES-5 b is from Ivshina & Winn (2022). Their analysis, which includes TESS data, found the period to be changing at a rate -17.47 ± 3.79 ms yr^{-1}.

The first analysis of the TrES-5 b ETD transit centers indicates the period could be changing at a rate of -29.7 ± 3.6 ms yr^{-1}, with the quadratic orbital decay model favored over a constant period by a ΔBIC of 26.8 (Table 1). The ETD hosts 268 transits of TrES-5 b from the years 2012–2021, 233 of which are DQ 1–3. There are no literature observations of TrES-5 b on the database. After removal of partial and duplicate transits there are 110 remaining (Table B1). The analysis of these cleaned data showed an increase in the best-fit period derivative to -34.5 ± 4.6 ms yr^{-1} in the orbital decay model, favored over a constant period by a ΔBIC of 22.2 (Table 3). The quadratic model is also a better fit to the data than the apsidal precession model by a difference ΔBIC = 10.1 (see Figure 3). The best-fit precession rate is $0.00058^{+0.00021}_{-0.00014}$ rad per epoch with an eccentricity $0.0098^{+0.0068}_{-0.0045}$ (Table A6).

5.6. TrES-1 b

TrES-1 b is a 0.7 M_J, 1.1 R_J HJ on a $3.03006973 \pm 0.00000018$ days orbit (Alonso et al. 2004; Bonomo et al. 2017). TrES-1 b was discovered in 2004, the first of the Trans-Atlantic Exoplanet Survey (TrES), and thus has one of the longest potential observational baselines in this study. It has been the subject of various short-term TTV studies in the past (Rabus et al. 2008, 2009; Baluev et al. 2015), but no significant variations were detected. Most recently Ivshina & Winn (2022) have included TESS data and found the TrES-1 b period to be changing at a rate -18.36 ± 3.73 ms yr^{-1}. As this was part of a much larger study they did not go into further detail but suggest the system is worth monitoring.

The ETD hosts 223 observations of TrES-1 b spanning the years 2004–2021, 169 of which are DQ 1–3. Prior to any data cleaning, the ETD transit times fit an orbital decay model with a period derivative of -7.9 ± 1.4 ms yr^{-1}, preferred over a linear ephemeris by ΔBIC of 9.9 (Table 1). The TrES-1 b system has the weakest evidence of a nonlinear timing trend out of the top eight systems picked from Table 1, but the results still fit the criteria for strong evidence with a ΔBIC > 5. Nineteen of the TrES-1 b transit times on the database are from published literature studies, though it was discovered that five of them are duplicates and were excluded. In addition, the observations from Hrudková et al. (2008) had to be converted from BJD_{UTC} to BJD_{TDB}. After these considerations, there are 68 remaining observations (Table B1).

The final analysis of the cleaned TrES-1 b data (see Figure 3) yields a best-fit period derivative of -10.9 ± 2.1 ms yr^{-1} with the orbital decay model being favored over a constant period by a ΔBIC of 9.7 (Table 3). Thus, the results of the second analysis are consistent with the first, which contained data duplicates and observations with inconsistent time stamps, suggesting the fit results are robust (Table A3). The BIC values for the constant-period and apsidal precession models are almost indistinguishable (Table A3). The best-fit apsidal precession model gives an eccentricity of $0.0030^{+0.0037}_{-0.0015}$ and a precession rate of $0.00057^{+0.00024}_{-0.00019}$ rad per epoch.

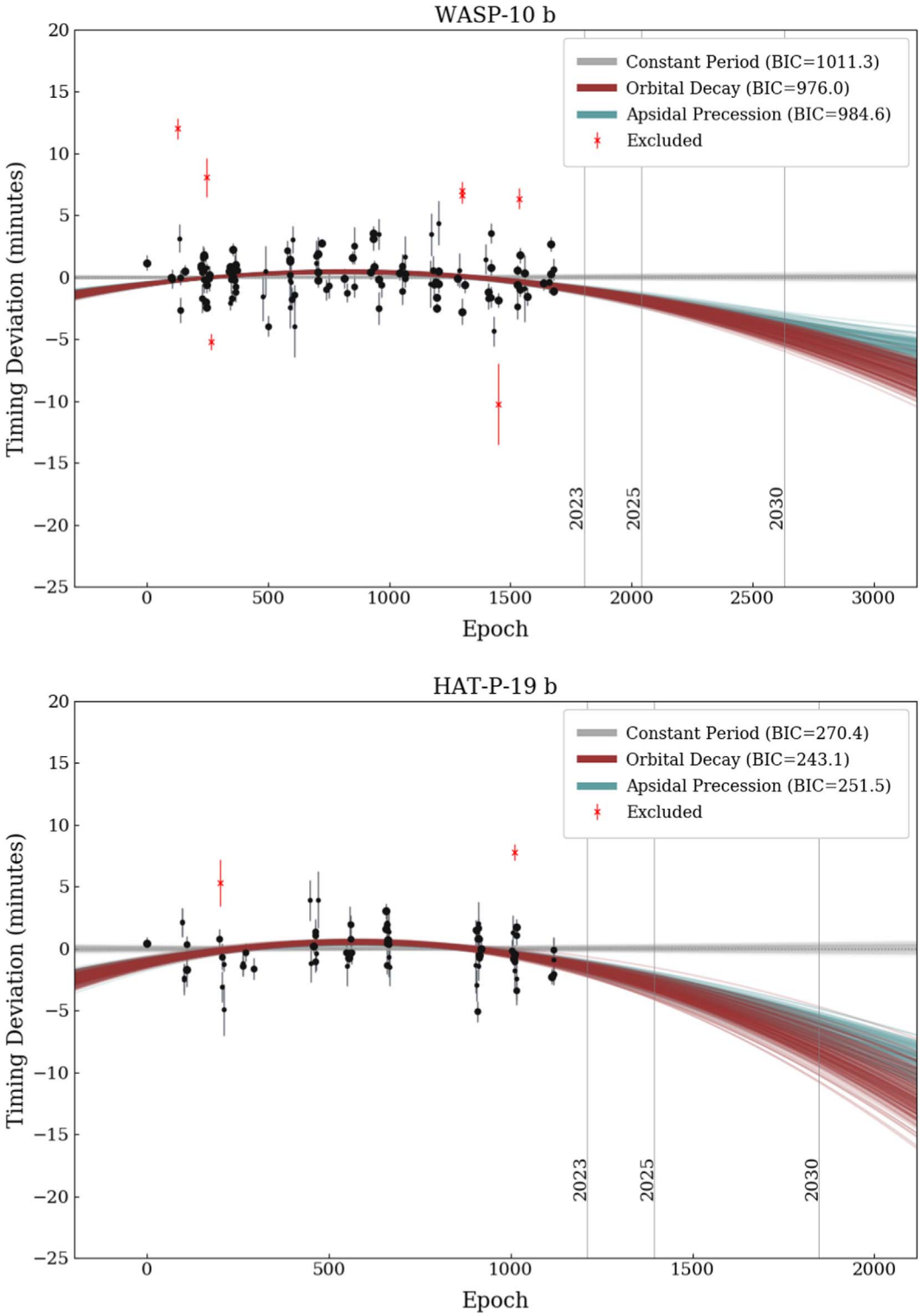

Figure 2. Similar to Figure 1, but for WASP-10 b (top) and HAT-P-19 b (bottom).

5.7. *TrES-2 b*

TrES-2 b is a 1.2 M_J, 1.2 R_J HJ discovered in 2006 on a $2.470613374 \pm 0.000000019$ days, near-grazing orbit (O'Donovan et al. 2006; Bonomo et al. 2017). As TrES-2 b lies within the Kepler field, it was extensively studied in the years following its discovery. Early publications suggest evidence of short-term transit timing and duration variations, with explanations including a third body in the system or the existence of a moon (Mislis & Schmitt 2009; Rabus et al. 2009). Later studies, however, were not able to support these claims, thus citing no evidence of short or long-term TTVs for TrES-2 b (Kipping & Bakos 2011; Schröter et al. 2012; Raetz et al. 2014). We have not found any TTV studies of TrES-2 b in years since.

The initial analysis of the TrES-2 b ETD data showed a strong preference for the orbital decay model with a period derivative of -20.7 ± 2.1 ms yr^{-1} (Table 1). The ΔBIC favors

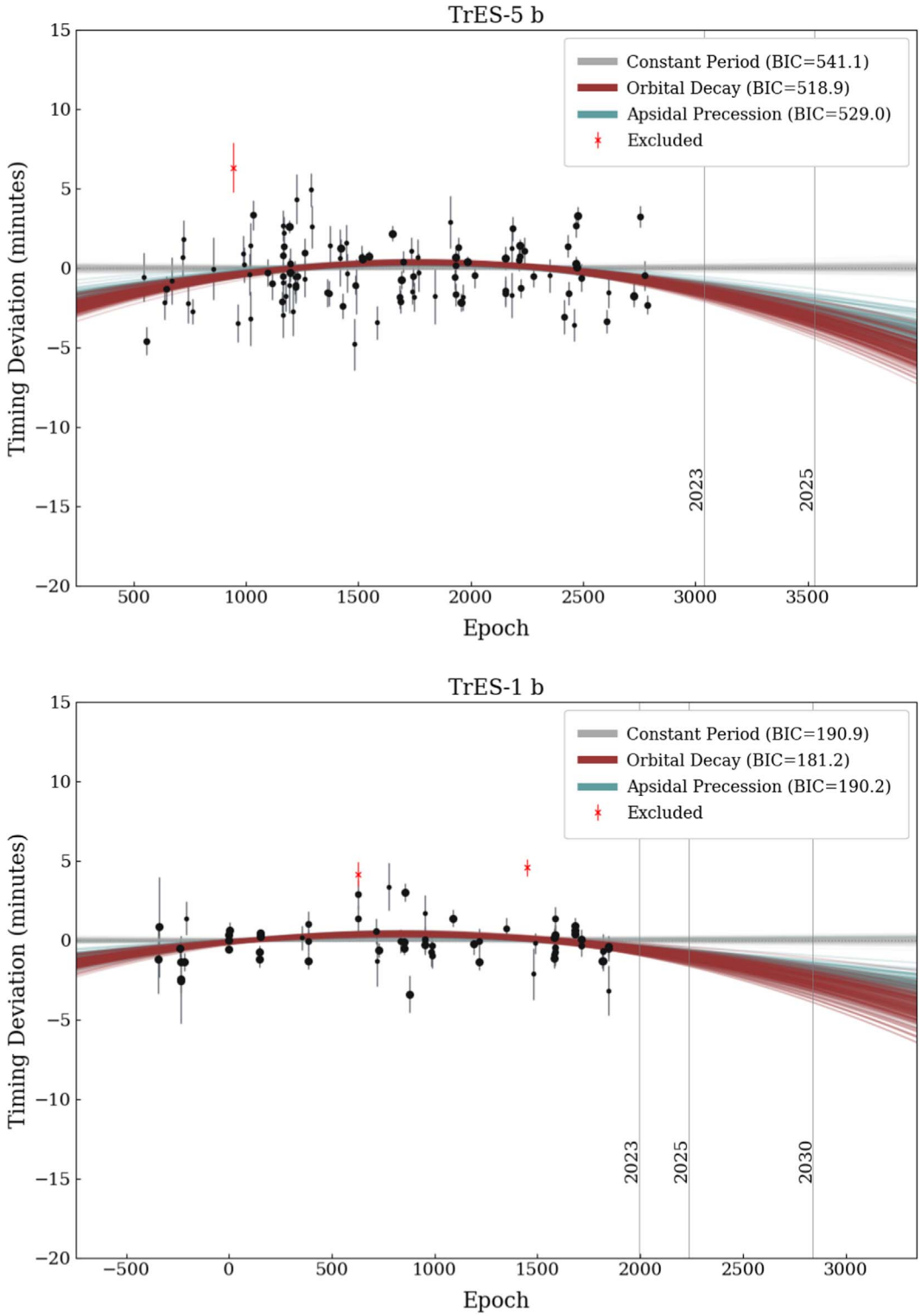

Figure 3. Similar to Figure 1, but for TrES-5 b (top) and TrES-1 b (bottom).

the decay model over a constant period by a significant value of 46.8. Because of this, TrES-2 b was selected as a target of interest for further analysis. The ETD hosts 331 transits of TrES-2 b spanning the years 2006–2021, 270 of which are DQ 1–3. After removal of partial and duplicate transits 152 remain (Table B1), as many were partial transits. The analysis of these cleaned data yields a less convincing, but still notable, argument for the decay scenario. It is worth highlighting that the first few epochs are mostly literature observations, which may be driving the model due to their generally higher precision and having been measured several years before the ETD observations begin (Figure 4). The ΔBIC favors the decay model over a linear ephemeris by 8.3, with the best-fit decay rate being -12.6 ± 2.4 ms yr^{-1} (Table 3).

Though the ΔBIC metric favors the orbital decay model over a constant period, it does not favor the apsidal precession

model over a constant period. If there is statistically significant curvature in the timing residuals, it is reasonable to expect that the apsidal precession model should be a better fit than a constant period. Looking at only the χ^2 values, the constant-period model ($\chi^2 = 868.8$) is a worse fit than both the apsidal precession ($\chi^2 = 857.4$) and orbital decay ($\chi^2 = 855.6$) models. The distinction between the two timing models is less clear in the case of TrES-2 b than for the other systems explored here due to the large spread in the ETD data and the high number of DQ 3 observations (Figure 4). We found that TrES-2 b was the only target that could not pass the MCMC convergence criteria for the apsidal precession model. The resulting best-fit apsidal precession rate and eccentricity are $0.00061^{+0.00023}_{-0.00022}$ rad per epoch and $0.0030^{+0.0039}_{-0.0014}$, respectively (Table A4).

5.8. HAT-P-32 b

HAT-P-32 b is a 0.8 M_J, 1.8 R_J HJ discovered in 2011 on a $2.15000825 \pm 0.00000012$ days orbit (Hartman et al. 2011b; Bonomo et al. 2017). In 2014 it was the subject of a TTV study seeking evidence of an additional body in the system, but amplitudes of greater than 1.5 minutes were ruled out (Seeliger et al. 2014). The contributed observations on the ETD span the years 2007–2021, though there is a 633 orbit gap after the discovery transit. During a preliminary examination of the HAT-P-32 b transit centers it was noted that, without the discovery epoch, there is visual curvature in the timing residuals.[13] This point was removed for the initial round of analysis so that the significance of the curvature could be examined and compared with other systems. HAT-P-32 b was selected for further analysis, as orbital decay at a rate of -30.2 ± 3.3 ms yr^{-1} is favored over a constant-period ephemeris by $\Delta\mathrm{BIC} = 39.7$ (Table 1).

The ETD hosts 167 transits of HAT-P-32 b, 142 of which are DQ 1–3. After the exclusion of partial and duplicate transits, 88 observations remain (Table B1). This includes the discovery epoch, which was added back to the data set as it was found that the transit time was not converted from $\mathrm{BJD_{UTC}}$ to $\mathrm{HJD_{UTC}}$ when listed on the database (Hartman et al. 2011b). Results from the final analysis of the cleaned HAT-P-32 b data maintain a preference for the orbital decay model over a constant period by a ΔBIC of 7.4, as well as the apsidal precession model by a ΔBIC of 9.4 (Figure 4). However, the χ^2 of the orbital decay and apsidal precession models are indistinguishable. The best-fit period derivative for the decay model is -7.3 ± 1.5 ms yr^{-1}, and the apsidal precession model yields an eccentricity of $0.0022^{+0.0049}_{-0.0012}$ and a precession rate of $0.00054^{+0.00028}_{-0.00024}$ rad epoch^{-1} (Table A2).

5.9. TrES-3 b

TrES-3 b is a 1.8 M_J, 1.3 R_J HJ with an orbital period of $1.306186483 \pm 0.00000007$ days that was discovered in 2007 (Bonomo et al. 2017; O'Donovan et al. 2007). It has been extensively studied in the search for periodic TTVs indicating the presence of another planet, but no conclusive evidence of such variations have been found (Gibson et al. 2009; Sozzetti et al. 2009; Jiang et al. 2013; Vanko et al. 2013; Püsküllü et al. 2017). Zhao et al. (2018) and Mannaday et al. (2020) have investigated the possibility of orbital decay, both concluding that TrES-3 b transit times are consistent with a constant period. However, Mannaday et al. (2020) found the difference in BIC values of the orbital decay and constant-period models to be very similar and recommend further observations.

The ETD hosts 556 observations of TrES-3 b from the years 2007–2021, 465 of which are DQ 1–3. This is one of the longest and most complete observational baselines in this study. In the initial round of analysis the orbital decay model was favored for TrES-3 b by a ΔBIC of 26.7 when compared to the linear model (Table 1). The best-fit decay rate is small at -5.08 ± 0.63 ms yr^{-1}, but it was selected for further analysis. Many of the observations of TrES-3 b on the ETD do not have a clear ingress or egress and many of the early observations do not have a recorded timing uncertainty, resulting in their immediate exclusion. After the removal of partial transits and duplicates (including the first literature observation) there are 231 observations remaining (Table B1). The second, follow-up analysis on this cleaned data set is more favorable toward a constant-period model (Figure 5). The best-fit decay rate is -2.75 ± 0.78 ms yr^{-1}, consistent with a constant period when considering the variance in the data. The BIC values for the decay and constant-period models are indistinguishable (Table 3). The precession model is strongly disfavored by its BIC, which can be explained by the apparent lack of curvature in the timing residuals. Indeed, the precession model is driven to a very low eccentricity of 0.0005 and a slow precession rate of 0.00013 rad per epoch, and is ultimately a poor fit (Table A5).

5.10. WASP-43 b

WASP-43 b is a 2.1 M_J, 1.0 R_J HJ on a $0.81347437 \pm 0.00000013$ day orbit (Hellier et al. 2011; Bonomo et al. 2017). The WASP-43 b system has been monitored since 2014 for signs of long-term TTVs because its ultrashort orbital period is thought to make it a good candidate for exhibiting orbital decay (Blecic et al. 2014; Chen et al. 2014; Murgas et al. 2014; Ricci et al. 2015). In 2016, Jiang et al. (2016) detected evidence of orbital decay at a rate of $-0.02890795 \pm 0.00772547$ s yr^{-1}. Later that same year, Hoyer et al. (2016) published a homogeneous analysis including new data that showed no indication of a period variation. Two years later, Zhao et al. (2018) found that orbital decay is slightly preferred over a constant period, but at a rate of -0.005248 ± 0.001714 s yr^{-1}. In this study, the initial analysis of ETD transit centers strongly favors a constant period (Table 1), but the system was selected for further analysis due to the interest in the literature.

The ETD hosts 186 transits of WASP-43 b spanning the years 2010–2021, with 162 being DQ 1–3. After the exclusion of partial and duplicate transits there are 126 remaining observations (Table B1). Analysis of the cleaned data supports the constant-period model for WASP-43 b over orbital decay by ΔBIC of 4.4 (Figure 5). In addition to this, the best-fit orbital decay rate is -1.0 ± 1.2 ms yr^{-1}, which is consistent with a constant orbital period (Table 3). Like TrES-3 b, apsidal precession results in poor fit due to the sinusoidal nature of the model and the strong linearity of the data (Table A10).

6. Discussion and Conclusions

This study has utilized the wealth of citizen science observations on the ETD to identify HJ systems that are

[13] http://var2.astro.cz/ETD/etd.php?STARNAME=HAT-P-32&PLANET=b

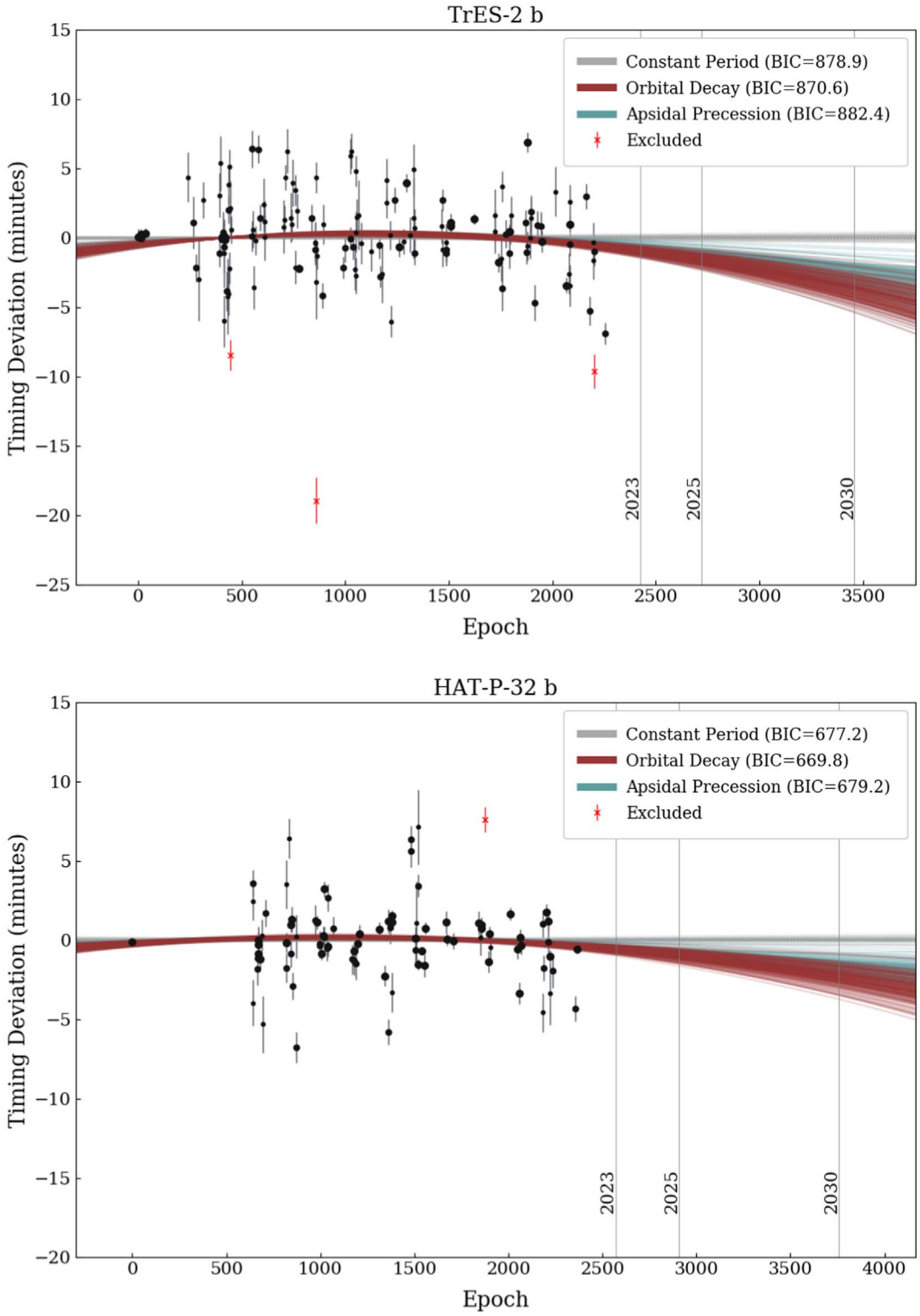

Figure 4. Similar to Figure 1, but for TrES-2 b (top) and HAT-P-32 b (bottom).

candidates for the detection of orbital decay, or more precisely, detectable period drifts. In the process, we have demonstrated the potential of citizen scientists to contribute to the detection of long-term orbital evolution signatures of close-in giant planets.

We highlight systems in the ETD that should be prioritized for further study in Table 3. We find that eight star–planet systems in the ETD show statistically compelling quadratic trends in the transit times and particularly recommend future follow-up of HAT-P-19 b, HAT-P-32 b, TrES-1 b, and WASP-10 b.

For an additional approach, we purposefully take a pessimistic view of the data's predictive power and assume that the uncertainties of the ETD transit centers are generally unreliable. In this case, we use the variance of the timing residuals during fitting and find that three of the targets

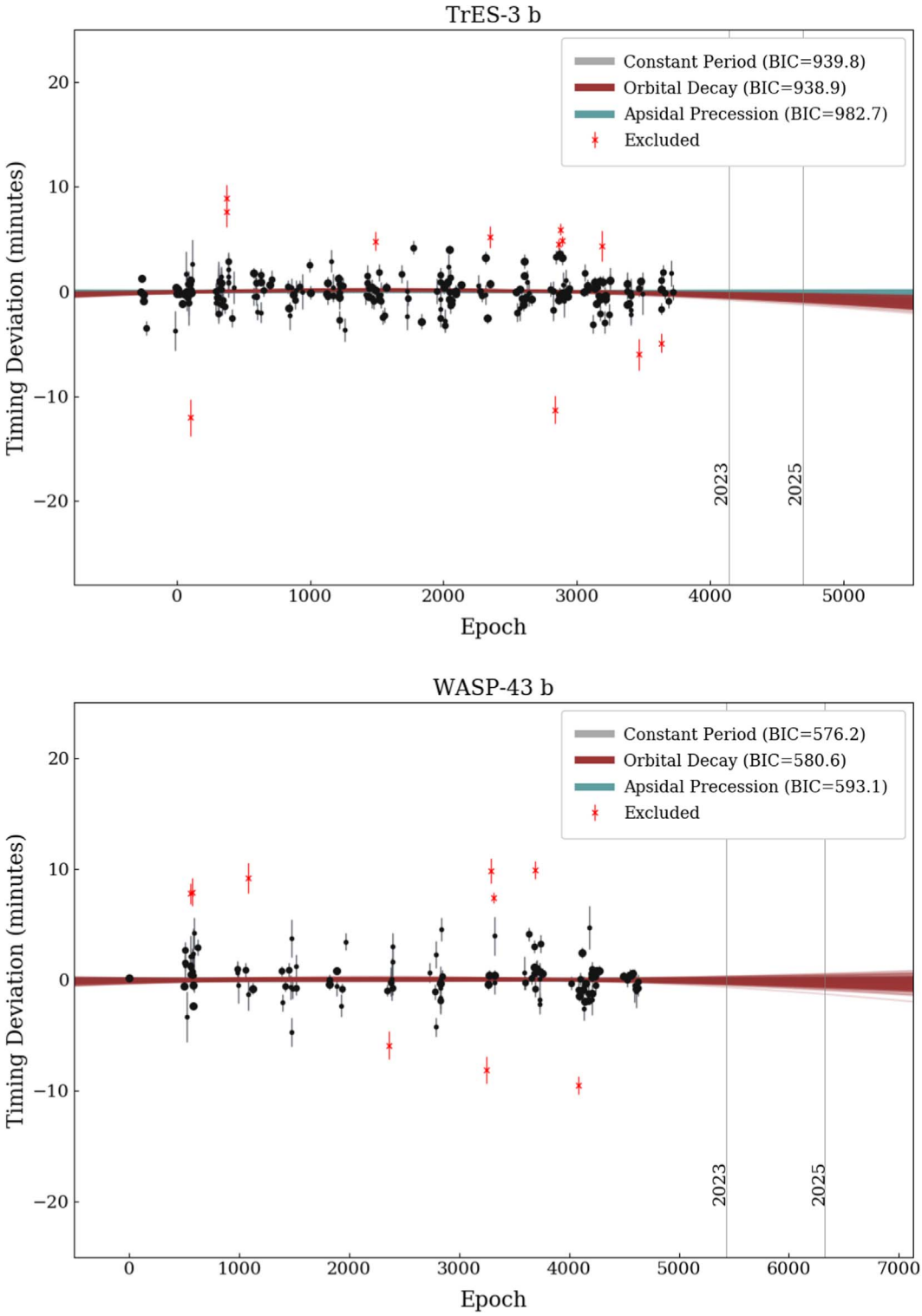

Figure 5. Similar to Figure 1, but for TrES-3 b (top) and WASP-43 b (bottom).

(WASP-12 b, HAT-P-19 b, and TrES-1 b) still show evidence of a negative period derivative.

In addition to orbital decay, we consider apsidal precession as a source of timing variations—in no case is this model preferred over orbital decay. In many cases, however, the χ^2 value of the orbital decay and apsidal precession models are similar. We further note that only the low-eccentricity ($e \ll 0.1$) expansion for precession is used in this work (as well as typically in others). Preliminary analysis of WASP-12 b using the higher-order eccentricity expansion for precession, up to e^5 as presented in Ragozzine & Wolf (2009), does show promise in fitting the data, but only if a high eccentricity ($e \approx 0.1$) is used. The overall results are also not clearly better than the orbital decay model and so are not pursued further here.

Confirmation of period drifts, regardless of the cause, would provide additional constraints on the system. For orbital decay, the period derivative can be used to infer properties such as the

planet's remaining lifetime and the stellar tidal dissipation rate. For precession, the model could constrain the interior density distribution of HJs and potentially yield an upper limit on orbital eccentricities (of course, radial velocity data, if available, provide independent eccentricity constraints). Other possible effects, such as line-of-sight acceleration and stellar activity, will also need to be considered in understanding the underlying cause of observed timing deviations.

As our study aims to aid in selecting systems for long-term observing campaigns, in addition to extending the observed baselines of those systems, a next step is to conduct in-depth analyses into the identified candidates. Such studies should combine all available data sets for the system of interest, homogeneously refitting them where possible. We will aim to conduct such studying, also seeking to obtain further observations of these systems, particularly by collaborating with citizen scientists.

WASP-12 b has proved to be critical as a control for this study and serves as an important test case for orbital decay searches in general. The consistency between the results using citizen science data and those in the literature demonstrates the feasibility of such work. The ETD offers a rich history of transit times for hundreds of star–planet systems that can make the search for evidence of long-term dynamical evolution, orbital decay in this case, more efficient. While this work does not suggest that any of the identified systems, apart from WASP-12 b, are indeed undergoing orbital decay or other period deviations, the results do suggest that there is sufficient evidence to keep looking.

This work would not be possible without the dedication and skill of the Exoplanet Transit Database (ETD) coordinators and observers, and we sincerely thank them all for their ongoing contributions. The names of observers of the data used for this study—as given on ETD with minor formatting changes—can be found in Table B1 and in the supplementary data tables on Zenodo:10.5281/zenodo.7098460. As of 2022 May 13 there are 625 ETD contributors consisting of universities, teams, and individuals from around the world. Additionally, this network of observers expands with the inclusion of the ExoClock and Exoplanet Watch programs. We emphasize the science potential of such a large community of ground-based observers, and encourage continued collaboration and the inclusion of new observers. Having identified key systems to follow-up in further depth, we look forward to collaborating with the participants of these programs as we continue to investigate the potential for nonlinear ephemerides.

We thank Darin Ragozzine for helpful comments on the draft of this paper. This work is supported, in part, by an NSERC Discovery Grant, an NSERC CREATE grant, and the Canada Research Chairs program. B.E. is a Laureate of the Paris Region fellowship program which is supported by the Ile-de-France Region and has received funding under the Horizon 2020 innovation framework program and the Marie Sklodowska-Curie grant agreement No. 945298.

Appendix A
Full MCMC Results

The results of the Metropolis–Hastings MCMC sampling of the constant-period, orbital decay, and apsidal precession transit-timing models are presented below. The top 10 targets of interest, as discussed in Section 5, are listed alphabetically. These are HAT-P-19 b, HAT-P-32 b, TrES-1 b, TrES-2 b, TrES-3 b, TrES-5 b, WASP-4 b, WASP-10 b, WASP-12 b, and WASP-43 b.

Table A1
HAT-P-19 b Results

Parameter	Symbol	Unit	Value	Uncertainty (1σ)
Constant period				
Transit center	t_0	$\mathrm{BJD_{TDB}}$	2455091.53464	$^{+0.00010}_{-0.00010}$
Period	P	days	4.00878388	$^{+0.00000015}_{-0.00000014}$
Number of data	n		72	
Degrees of freedom	k		2	
Chi-square statistic	χ^2		261.8	
Bayesian information criterion	BIC		270.4	
Orbital decay				
Transit center	t_0	$\mathrm{BJD_{TDB}}$	2455091.53382	$^{+0.00014}_{-0.00015}$
Period	P	days	4.00878805	$^{+0.00000055}_{-0.00000054}$
Decay rate	dP/dE	days epoch^{-1}	-7.33×10^{-9}	$^{+0.92\times10^{-9}}_{-0.93\times10^{-9}}$
Decay rate	dP/dt	ms yr^{-1}	-57.7	$^{+7.2}_{-7.3}$
Degrees of freedom	k		3	
Chi-square statistic	χ^2		230.3	
Bayesian information criterion	BIC		243.1	
Apsidal precession				
Transit center	t_0	$\mathrm{BJD_{TDB}}$	2455091.5263	$^{+0.0013}_{-0.0011}$
Sidereal period	P_s	days	4.00878386	$^{+0.00000014}_{-0.00000014}$
Argument of periastron	ω_0	rad	2.623	$^{+0.046}_{-0.043}$
Precession rate	$d\omega/dE$	rad epoch^{-1}	0.000905	$^{+0.000059}_{-0.000068}$
Eccentricity	e		0.0068	$^{+0.0009}_{-0.0010}$
Degrees of freedom	k		5	
Chi-square statistic	χ^2		230.1	
Bayesian information criterion	BIC		251.5	

Table A2
HAT-P-32 b Results

Parameter	Symbol	Unit	Value	Uncertainty (1σ)
Constant period				
Transit center	t_0	$\mathrm{BJD_{TDB}}$	2454420.447196	$^{+0.000052}_{-0.000051}$
Period	P	days	2.150008203	$^{+0.000000038}_{-0.000000038}$
Number of data	n		87	
Degrees of freedom	k		2	
Chi-square statistic	χ^2		668.3	
Bayesian information criterion	BIC		677.2	
Orbital decay				
Transit center	t_0	$\mathrm{BJD_{TDB}}$	2454420.447035	$^{+0.000061}_{-0.000061}$
Period	P	days	2.15000874	$^{+0.00000012}_{-0.00000012}$
Decay rate	dP/dE	days epoch^{-1}	-0.50×10^{-9}	$^{+0.10\times10^{-9}}_{-0.10\times10^{-9}}$
Decay rate	dP/dt	ms yr^{-1}	-7.3	$^{+1.5}_{-1.5}$
Degrees of freedom	k		3	
Chi-square statistic	χ^2		656.4	
Bayesian information criterion	BIC		669.8	
Apsidal precession				
Transit center	t_0	$\mathrm{BJD_{TDB}}$	2454420.4458	$^{+0.0008}_{-0.0034}$
Sidereal period	P_s	days	2.150008198	$^{+0.000000037}_{-0.000000037}$
Argument of periastron	ω_0	rad	2.55	$^{+0.27}_{-0.34}$
Precession rate	$d\omega/dE$	rad epoch^{-1}	0.00054	$^{+0.00028}_{-0.00024}$
Eccentricity	e		0.0022	$^{+0.0049}_{-0.0012}$
Degrees of freedom	k		5	
Chi-square statistic	χ^2		656.8	
Bayesian information criterion	BIC		679.2	

Table A3
TrES-1 b Results

Parameter	Symbol	Unit	Value	Uncertainty (1σ)
Constant period				
Transit center	t_0	$\mathrm{BJD_{TDB}}$	2453898.874169	$^{+0.000038}_{-0.000038}$
Period	P	days	3.030069676	$^{+0.000000042}_{-0.000000042}$
Number of data	n		66	
Degrees of freedom	k		2	
Chi-square statistic	χ^2		182.6	
Bayesian information criterion	BIC		190.9	
Orbital decay				
Transit center	t_0	$\mathrm{BJD_{TDB}}$	2453898.874084	$^{+0.000041}_{-0.000041}$
Period	P	days	3.03007055	$^{+0.00000017}_{-0.00000017}$
Decay rate	dP/dE	days/epoch	-1.05×10^{-9}	$^{+0.20\times10^{-9}}_{-0.20\times10^{-9}}$
Decay rate	dP/dt	ms yr^{-1}	-10.9	$^{+2.1}_{-2.0}$
Degrees of freedom	k		3	
Chi-square statistic	χ^2		168.6	
Bayesian information criterion	BIC		181.2	
Apsidal precession				
Transit center	t_0	$\mathrm{BJD_{TDB}}$	2453898.8715	$^{+0.0015}_{-0.0035}$
Sidereal period	P_s	days	3.030069678	$^{+0.000000042}_{-0.000000042}$
Argument of periastron	ω_0	rad	2.67	$^{+0.15}_{-0.20}$
Precession rate	$d\omega/dE$	rad epoch^{-1}	0.00057	$^{+0.00024}_{-0.00019}$
Eccentricity	e		0.0030	$^{+0.0037}_{-0.0015}$
Degrees of freedom	k		5	
Chi-square statistic	χ^2		169.2	
Bayesian information criterion	BIC		190.2	

Table A4
TrES-2 b Results

Parameter	Symbol	Unit	Value	Uncertainty (1σ)
Constant period				
Transit center	t_0	$\mathrm{BJD_{TDB}}$	2453957.635474	$^{+0.000020}_{-0.000020}$
Period	P	days	2.47061340	$^{+0.000000042}_{-0.000000042}$
Number of data	n		149	
Degrees of freedom	k		2	
Chi-square statistic	χ^2		868.8	
Bayesian information criterion	BIC		878.9	
Orbital decay				
Transit center	t_0	$\mathrm{BJD_{TDB}}$	2453957.635119	$^{+0.000069}_{-0.000070}$
Period	P	days	2.47061447	$^{+0.00000020}_{-0.00000020}$
Decay rate	dP/dE	days epoch^{-1}	-0.99×10^{-9}	$^{+0.18\times10^{-9}}_{-0.19\times10^{-9}}$
Decay rate	dP/dt	ms yr^{-1}	-12.6	$^{+2.4}_{-2.4}$
Degrees of freedom	k		3	
Chi-square statistic	χ^2		855.6	
Bayesian information criterion	BIC		870.6	
Apsidal precession				
Transit center	t_0	$\mathrm{BJD_{TDB}}$	2453957.6333	$^{+0.0011}_{-0.0031}$
Sidereal period	P_s	days	2.470613392	$^{+0.000000042}_{-0.000000042}$
Argument of periastron	ω_0	rad	2.47	$^{+0.24}_{-0.26}$
Precession rate	$d\omega/dE$	rad epoch^{-1}	0.00061	$^{+0.00023}_{-0.00022}$
Eccentricity	e		0.0030	$^{+0.0039}_{-0.0014}$
Degrees of freedom	k		5	
Chi-square statistic	χ^2		857.4	
Bayesian information criterion	BIC		882.4	

Table A5
TrES-3 b Results

Parameter	Symbol	Unit	Value	Uncertainty (1σ)
Constant period				
Transit center	t_0	$\mathrm{BJD_{TDB}}$	2454538.581479	$^{+0.000027}_{-0.000027}$
Period	P	days	1.306186320	$^{+0.000000014}_{-0.000000014}$
Number of data	n		218	
Degrees of freedom	k		2	
Chi-square statistic	χ^2		929.0	
Bayesian information criterion	BIC		939.8	
Orbital decay				
Transit center	t_0	$\mathrm{BJD_{TDB}}$	2454538.581437	$^{+0.000030}_{-0.000030}$
Period	P	days	1.306186497	$^{+0.000000050}_{-0.000000052}$
Decay rate	dP/dE	days epoch^{-1}	-0.11×10^{-9}	$^{+0.032\times10^{-9}}_{-0.031\times10^{-9}}$
Decay rate	dP/dt	ms yr^{-1}	-2.75	$^{+0.78}_{-0.76}$
Degrees of freedom	k		3	
Chi-square statistic	χ^2		922.8	
Bayesian information criterion	BIC		938.9	
Apsidal precession				
Transit center	t_0	$\mathrm{BJD_{TDB}}$	2454538.58143	$^{+0.00010}_{-0.00055}$
Sidereal period	P_s	days	1.306186320	$^{+0.000000011}_{-0.000000011}$
Argument of periastron	ω_0	rad	2.5	$^{+2.0}_{-1.0}$
Precession rate	$d\omega/dE$	rad epoch^{-1}	0.00013	$^{+0.00052}_{-0.00012}$
Eccentricity	e		0.0005	$^{+0.0027}_{-0.0005}$
Degrees of freedom	k		5	
Chi-square statistic	χ^2		955.8	
Bayesian information criterion	BIC		982.7	

Table A6
TrES-5 b Results

Parameter	Symbol	Unit	Value	Uncertainty (1σ)
Constant period				
Transit center	t_0	$\mathrm{BJD_{TDB}}$	2455443.25340	$^{+0.00012}_{-0.00012}$
Period	P	days	1.482246663	$^{+0.000000064}_{-0.000000064}$
Number of data	n		109	
Degrees of freedom	k		2	
Chi-square statistic	χ^2		531.8	
Bayesian information criterion	BIC		541.1	
Orbital decay				
Transit center	t_0	$\mathrm{BJD_{TDB}}$	2455443.25109	$^{+0.00033}_{-0.00032}$
Period	P	days	1.48224954	$^{+0.00000038}_{-0.00000039}$
Decay rate	dP/dE	days epoch^{-1}	-1.6×10^{-9}	$^{+0.22\times10^{-09}}_{-0.21\times10^{-09}}$
Decay rate	dP/dt	ms yr^{-1}	-34.5	$^{+4.6}_{-4.5}$
Degrees of freedom	k		3	
Chi-square statistic	χ^2		504.9	
Bayesian information criterion	BIC		518.9	
Apsidal precession				
Transit center	t_0	$\mathrm{BJD_{TDB}}$	2455443.2490	$^{+0.0021}_{-0.0032}$
Sidereal period	P_s	days	1.482246666	$^{+0.000000064}_{-0.000000064}$
Argument of periastron	ω_0	rad	2.11	$^{+0.24}_{-0.37}$
Precession rate	$d\omega/dE$	rad epoch^{-1}	0.00058	$^{+0.00021}_{-0.00014}$
Eccentricity	e		0.0098	$^{+0.0068}_{-0.0045}$
Degrees of freedom	k		5	
Chi-square statistic	χ^2		505.6	
Bayesian information criterion	BIC		529.0	

Table A7
WASP-4 b Results

Parameter	Symbol	Unit	Value	Uncertainty (1σ)
Constant period				
Transit center	t_0	$\mathrm{BJD_{TDB}}$	2455880.794607	$^{+0.000018}_{-0.000018}$
Period	P	days	1.338231560	$^{+0.000000016}_{-0.000000015}$
Number of data	n		55	
Degrees of freedom	k		2	
Chi-square statistic	χ^2		396.9	
Bayesian information criterion	BIC		404.9	
Orbital decay				
Transit center	t_0	$\mathrm{BJD_{TDB}}$	2455880.794814	$^{+0.000029}_{-0.000029}$
Period	P	days	1.338231695	$^{+0.000000022}_{-0.000000022}$
Decay rate	dP/dE	days epoch^{-1}	-0.263×10^{-9}	$^{+0.029\times10^{-9}}_{-0.029\times10^{-9}}$
Decay rate	dP/dt	ms yr^{-1}	-6.21	$^{+0.70}_{-0.70}$
Degrees of freedom	k		3	
Chi-square statistic	χ^2		357.4	
Bayesian information criterion	BIC		369.5	
Apsidal precession				
Transit center	t_0	$\mathrm{BJD_{TDB}}$	2455880.7937	$^{+0.0007}_{-0.0033}$
Sidereal period	P_s	days	1.338231569	$^{+0.000000018}_{-0.000000017}$
Argument of periastron	ω_0	rad	2.95	$^{+0.074}_{-0.089}$
Precession rate	$d\omega/dE$	rad epoch^{-1}	0.00048	$^{+0.00040}_{-0.00024}$
Eccentricity	e		0.0027	$^{+0.0079}_{-0.0017}$
Degrees of freedom	k		5	
Chi-square statistic	χ^2		358.8	
Bayesian information criterion	BIC		378.8	

Table A8
WASP-10 b Results

Parameter	Symbol	Unit	Value	Uncertainty (1σ)
Constant period				
Transit center	t_0	BJD_{TDB}	2454357.857968	$^{+0.000031}_{-0.000031}$
Period	P	days	3.092728113	$^{+0.000000044}_{-0.000000044}$
Number of data	n		122	
Degrees of freedom	k		2	
Chi-square statistic	χ^2		1001.7	
Bayesian information criterion	BIC		1011.3	
Orbital decay				
Transit center	t_0	BJD_{TDB}	2454357.857571	$^{+0.000054}_{-0.000054}$
Period	P	days	3.09272986	$^{+0.00000020}_{-0.00000020}$
Decay rate	dP/dE	days epoch^{-1}	-2.15×10^{-9}	$^{+0.24\times10^{-09}}_{-0.24\times10^{-09}}$
Decay rate	dP/dt	ms yr^{-1}	-21.9	$^{+2.4}_{-2.4}$
Degrees of freedom	k		3	
Chi-square statistic	χ^2		961.6	
Bayesian information criterion	BIC		976.0	
Apsidal precession				
Transit center	t_0	BJD_{TDB}	2454357.8547	$^{+0.0010}_{-0.0026}$
Sidereal period	P_s	days	3.092728117	$^{+0.000000044}_{-0.000000044}$
Argument of periastron	ω_0	rad	2.51	$^{+0.16}_{-0.12}$
Precession rate	$d\omega/dE$	rad epoch^{-1}	0.00078	$^{+0.00015}_{-0.00020}$
Eccentricity	e		0.0037	$^{+0.0027}_{-0.0011}$
Degrees of freedom	k		5	
Chi-square statistic	χ^2		960.6	
Bayesian information criterion	BIC		984.6	

Table A9
WASP-12 b Results

Parameter	Symbol	Unit	Value	Uncertainty (1σ)
Constant period				
Transit center	t_0	BJD_{TDB}	2454508.978942	$^{+0.000046}_{-0.000047}$
Period	P	days	1.091419487	$^{+0.000000020}_{-0.000000020}$
Number of data	n		213	
Degrees of freedom	k		2	
Chi-square statistic	χ^2		2342.4	
Bayesian information criterion	BIC		2353.1	
Orbital decay				
Transit center	t_0	BJD_{TDB}	2454508.977198	$^{+0.000074}_{-0.000074}$
Period	P	days	1.091421946	$^{+0.000000084}_{-0.000000084}$
Decay rate	dP/dE	days epoch^{-1}	-1.093×10^{-9}	$^{+0.036\times10^{-09}}_{-0.036\times10^{-09}}$
Decay rate	dP/dt	ms yr^{-1}	-31.6	$^{+1.0}_{-1.0}$
Degrees of freedom	k		3	
Chi-square statistic	χ^2		1895.7	
Bayesian information criterion	BIC		1911.8	
Apsidal precession				
Transit center	t_0	BJD_{TDB}	2454508.9700	$^{+0.0014}_{-0.0008}$
Sidereal period	P_s	days	1.091419481	$^{+0.000000020}_{-0.000000020}$
Argument of periastron	ω_0	rad	2.382	$^{+0.031}_{-0.059}$
Precession rate	$d\omega/dE$	rad epoch^{-1}	0.000336	$^{+0.000026}_{-0.000013}$
Eccentricity	e		0.0287	$^{+0.0022}_{-0.0039}$
Degrees of freedom	k		5	
Chi-square statistic	χ^2		1902.6	
Bayesian information criterion	BIC		1929.4	

Table A10
WASP-43 b Results

Parameter	Symbol	Unit	Value	Uncertainty (1σ)
Constant period				
Transit center	t_0	$\mathrm{BJD_{TDB}}$	2455528.868421	$^{+0.000054}_{-0.000054}$
Period	P	days	0.813474243	$^{+0.000000017}_{-0.000000017}$
Number of data	n		116	
Degrees of freedom	k		2	
Chi-square statistic	χ^2		566.6	
Bayesian information criterion	BIC		576.2	
Orbital decay				
Transit center	t_0	$\mathrm{BJD_{TDB}}$	2455528.868381	$^{+0.000072}_{-0.000072}$
Period	P	days	0.813474304	$^{+0.000000077}_{-0.000000072}$
Decay rate	dP/dE	days epoch^{-1}	-0.026×10^{-9}	$^{+0.031\times10^{-9}}_{-0.031\times10^{-9}}$
Decay rate	dP/dt	ms yr^{-1}	-1.0	$^{+1.2}_{-1.2}$
Degrees of freedom	k		3	
Chi-square statistic	χ^2		566.3	
Bayesian information criterion	BIC		580.6	
Apsidal precession				
Transit center	t_0	$\mathrm{BJD_{TDB}}$	2455528.86842	$^{+0.00015}_{-0.00013}$
Sidereal period	P_s	days	0.813474243	$^{+0.000000013}_{-0.000000013}$
Argument of periastron	ω_0	rad	3.1	$^{+2.2}_{-2.1}$
Precession rate	$d\omega/dE$	rad epoch^{-1}	0.000015	$^{+0.00015}_{-0.00001}$
Eccentricity	e		0.00024	$^{+0.0037}_{-0.0002}$
Degrees of freedom	k		5	
Chi-square statistic	χ^2		569.3	
Bayesian information criterion	BIC		593.1	

Appendix B
Exoplanet Transit Database (ETD) Observations

The final cleaned data sets for the 10 targets of interest (Section 5) are highlighted in Table B1 in a machine-readable format to ensure reproducibility of these results. Observer names are also listed, as given in the ETD with minor formatting changes. For entries where there are more than two observers, the full list of names is given in the table notes.

Table B1
ETD Transit Centers

Planet	Epoch	Transit Center (BJD_{TDB})	Error	Data Quality	Observer
HAT-P-19 b	0	2455091.534936	0.00034	1	Hartman et al.
HAT-P-19 b	97	2455480.388138842	0.00082	3	Ioannidis P., Avdellidou
HAT-P-19 b	97	2455480.388168842	0.00077	3	Lomoz F.
HAT-P-19 b	101	2455496.4200886358	0.00089	3	Naves R.
HAT-P-19 b	101	2455496.420158636	0.00072	3	Vanhuysse M.
HAT-P-19 b	108	2455524.482118315	0.00036	1	Muler G.
HAT-P-19 b	108	2455524.482168315	0.00103	3	Husar D.
HAT-P-19 b	109	2455528.492328273	0.00043	2	Ruiz J.
HAT-P-19 b	198	2455885.274367737	0.00056	2	Ayiomamitis A.

Note. Table B1 is published in its entirety in the machine-readable format. A portion is shown here for guidance regarding its form and content.

(This table is available in its entirety in machine-readable form.)

ORCID iDs

Simone R. Hagey https://orcid.org/0000-0001-8072-0590
Billy Edwards https://orcid.org/0000-0002-5494-3237
Aaron C. Boley https://orcid.org/0000-0002-0574-4418

References

Alonso, R., Brown, T. M., Torres, G., et al. 2004, ApJL, 613, L153
Baluev, R. V., Sokov, E. N., Hoyer, S., et al. 2020, MNRAS, 496, L11
Baluev, R. V., Sokov, E. N., Jones, H. R. A., et al. 2019, MNRAS, 490, 1294
Baluev, R. V., Sokov, E. N., Shaidulin, V. S., et al. 2015, MNRAS, 450, 3101
Barros, S. C. C., Boué, G., Gibson, N. P., et al. 2013, MNRAS, 430, 3032
Başẗurk, Ö., Yalçınkaya, S., Esmer, E. M., et al. 2020, MNRAS, 496, 4174
Batygin, K., Bodenheimer, P. H., & Laughlin, G. P. 2016, ApJ, 829, 114
Birkby, J. L., Cappetta, M., Cruz, P., et al. 2014, MNRAS, 440, 1470
Blecic, J., Harrington, J., Madhusudhan, N., et al. 2014, ApJ, 781, 116
Boley, A. C., Granados Contreras, A. P., & Gladman, B. 2016, ApJL, 817, L17
Bonomo, A. S., Desidera, S., Benatti, S., et al. 2017, A&A, 602, A107
Bouma, L. G., Winn, J. N., Baxter, C., et al. 2019, AJ, 157, 217
Bouma, L. G., Winn, J. N., Howard, A. W., et al. 2020, ApJL, 893, L29
Chen, G., van Boekel, R., Wang, H., et al. 2014, A&A, 563, A40
Christian, D. J., Gibson, N. P., Simpson, E. K., et al. 2009, MNRAS, 392, 1585
Collins, K. 2019, AAS Meeting Abstracts, 233, 140.05
Davoudi, F., MirshafieKhozani, P., Paki, E., et al. 2021, AstL, 47, 638
Eastman, J., Siverd, R., & Gaudi, B. S. 2010, PASP, 122, 935
Edwards, B., Anisman, L., Changeat, Q., et al. 2020, RNAAS, 4, 109
Edwards, B., Changeat, Q., Yip, K. H., et al. 2021, MNRAS, 504, 5671
Edwards, B., Ho, C. S. K., Osborne, H. L. M., et al. 2021, ATOM, 2, 25
Fabrycky, D., & Tremaine, S. 2007, ApJ, 669, 1298
Ford, E. B. 2006, ApJ, 642, 505
Foreman-Mackey, D., Hogg, D. W., Lang, D., & Goodman, J. 2013, PASP, 125, 306
Gibson, N. P., Pollacco, D., Simpson, E. K., et al. 2009, ApJ, 700, 1078
Hartman, J. D., Bakos, G. Á., Sato, B., et al. 2011a, ApJ, 726, 52
Hartman, J. D., Bakos, G. Á., Torres, G., et al. 2011b, ApJ, 742, 59
Hebb, L., Collier-Cameron, A., Loeillet, B., et al. 2008, ApJ, 693, 1920
Hellier, C., Anderson, D. R., Collier Cameron, A., et al. 2011, A&A, 535, L7
Hoyer, S., Pallé, E., Dragomir, D., & Murgas, F. 2016, AJ, 151, 137
Hrudková, M., Skillen, I., Benn, C., et al. 2008, in IAU Proc. 253, Transiting Planets (Cambridge: Cambridge Univ. Press), 446
Ioannidis, P., Huber, K. F., & Schmitt, J. 2016, A&A, 585, A72
Ivshina, E. S., & Winn, J. N. 2022, ApJSS, 259, 62
Jiang, I.-G., Lai, C.-Y., Savushkin, A., et al. 2016, AJ, 151, 17
Jiang, I.-G., Yeh, L.-C., Thakur, P., et al. 2013, AJ, 145, 68
Johnson, J. A., Winn, J. N., Cabrera, N. E., & Carter, J. A. 2009, ApJL, 692, L100
Johnson, J. A., Winn, J. N., Cabrera, N. E., & Carter, J. A. 2010, ApJL, 712, L122
Kipping, D., & Bakos, G. 2011, ApJ, 733, 36
Kokori, A., Tsiaras, A., Edwards, B., et al. 2021, ExA, 53, 547
Kokori, A., Tsiaras, A., Edwards, B., et al. 2022, ApJS, 258, 40
Levrard, B., Winisdoerffer, C., & Chabrier, G. 2009, ApJL, 692, L9
Liddle, A. R. 2007, MNRAS, 377, L74
Lin, D. N. C., Bodenheimer, P., & Richardson, D. C. 1996, Natur, 380, 606
Maciejewski, G., Dimitrov, D., Fernández, M., et al. 2016, A&A, 588, L6
Maciejewski, G., Dimitrov, D., Neuhäuser, R., et al. 2011a, MNRAS, 411, 1204
Maciejewski, G., Fernández, M., Aceituno, F., et al. 2021, A&A, 656, A88
Maciejewski, G., Raetz, S., Nettelmann, N., et al. 2011b, A&A, 535, A7
Maciejewski, G., Stangret, M., Ohlert, J., et al. 2018, IBVS, 63, 1
Mallonn, M., von Essen, C., Herrero, E., et al. 2019, A&A, 622, A81
Mandushev, G., Quinn, S. N., Buchhave, L.A., et al. 2011, ApJ, 741, 114
Mannaday, V. K., Thakur, P., Jiang, I.-G., et al. 2020, AJ, 160, 47
Matsumura, S., Peale, S. J., & Rasio, F. A. 2010, ApJ, 725, 1995
Mislis, D., & Schmitt, J. H. M. M. 2009, A&A, 500, L45
Murgas, F., Pallé, E., Zapatero Osorio, M. R., et al. 2014, A&A, 563, A41
O'Donovan, F. T., Charbonneau, D., Bakos, G. Á., et al. 2007, ApJL, 663, L37
O'Donovan, F. T., Charbonneau, D., Mandushev, G., et al. 2006, ApJL, 651, L61
Patra, K. C., Winn, J. N., Holman, M. J., et al. 2017, AJ, 154, 4
Patra, K. C., Winn, J. N., Holman, M. J., et al. 2020, AJ, 159, 150
Penev, K., Bouma, L. G., Winn, J. N., & Hartman, J. D. 2018, AJ, 155, 165
Petrucci, R., Jofré, E., Gómez Maqueo Chew, Y., et al. 2020, MNRAS, 491, 1243
Petrucci, R., Jofré, E., Schwartz, M., et al. 2013, ApJL, 779, L23
Poddaný, S., Brát, L., & Pejcha, O. 2010, NewA, 15, 297
Poddaný, S., Brát, L., & Pejcha, O. 2011, EPJ Web of Conferences, 11, 6008
Rabus, M., Alonso, R., Deeg, H. J., et al. 2008, in IAU Proc. 253, Transiting Planets (Cambridge: Cambridge Univ. Press), 432
Rabus, M., Deeg, H. J., Alonso, R., Belmonte, J. A., & Almenara, J. M. 2009, A&A, 508, 1011
Raetz, S., Maciejewski, G., Ginski, C., et al. 2014, MNRAS, 444, 1351
Ragozzine, D., & Wolf, A. S. 2009, ApJ, 698, 1778
Ricci, D., Ramón-Fox, F. G., Ayala-Loera, C., et al. 2015, PASP, 127, 143
Ricker, G. R., Winn, J. N., Vanderspek, R., et al. 2015, JATIS, 1, 014003
Schröter, S., Schmitt, J. H. M. M., & Müller, H. M. 2012, A&A, 539, A97
Seeliger, M., Dimitrov, D., Kjurkchieva, D., et al. 2014, MNRAS, 441, 304
Seeliger, M., Kitze, M., Errmann, R., et al. 2015, MNRAS, 451, 4060
Sokov, E. N., Sokova, I. A., Dyachenko, V. V., et al. 2018, MNRAS, 480, 291
Sonbas, E., Karaman, N., Özdönmez, A., et al. 2021, MNRAS, 509, 5102
Sousa-Silva, C., McKemmish, L. K., Chubb, K. L., et al. 2018, PhyEd, 53, 015020
Southworth, J., Dominik, M., Jørgensen, U. G., et al. 2019, MNRAS, 490, 4230
Püsküllü, Ç., Soydugan, F., Erdem, A., & Budding, E. 2017, NewA, 55, 39
Sozzetti, A., Torres, G., Charbonneau, D., et al. 2009, ApJ, 691, 1145
Tinetti, G., Drossart, P., Eccleston, P., et al. 2018, ExA, 46, 135
Tinetti, G., Eccleston, P., Haswell, C., et al. 2021, arXiv:2104.04824
Turner, J. D., Flagg, L., Ridden-Harper, A., & Jayawardhana, R. 2022, AJ, 163, 281
Turner, J. D., Ridden-Harper, A., & Jayawardhana, R. 2020, AJ, 161, 72
Vanko, M., Maciejewski, G., Jakubík, M., et al. 2013, MNRAS, 432, 944
Wilson, D. M., Gillon, M., Hellier, C., et al. 2008, ApJL, 675, L113
Wong, I., Shporer, A., Vissapragada, S., et al. 2022, AJ, 163, 175
Yee, S. W., Winn, J. N., Knutson, H. A., et al. 2019, ApJL, 888, L5
Zellem, R. T., Pearson, K. A., Blaser, E., et al. 2020, PASP, 132, 054401
Zhao, S., Jiang-hui, J., & Yao, D. 2018, ChA&A, 42, 101